SURFACE PRESSURE MEASUREMENTS AT TWO TIPS OF A MODEL HELICOPTER ROTOR IN HOVER

By R. B. Gray, H. M. McMahon, K. R. Shenoy

and M. L. Hammer

Prepared under Contract No. NAS1-15158 by

School of Aerospace Engineering

GEORGIA INSTITUTE OF TECHNOLOGY

Atlanta, Ga.

for

NATIONAL AERONAUTICS AND SPACE ADMINISTRATION

SUMMARY

Blade-tip surface pressure distribution data for a single-bladed, hovering, model helicopter rotor with two tip shapes are compared. The rotor had a constant-chord, untwisted blade with a square, flat tip and the pressure distributions on this blade are compared with those measured on the same blade with a half-body of revolution tip. Pressure measurements were made on each blade along the chordwise direction at six radial stations outboard of the 94 percent blade radius. Data on each blade were taken at blade collective pitch angles of 0, 6.18, and 11.4 degrees. The Reynolds number based on tip speed and blade chord was 736,000 and the tip Mach number was 0.25.

For a blade pitch angle of 0 degrees, a small difference in pressure distribution between the two blades occurred very near the tip.

For the pitch angles of 6.18 and 11.4 degrees, the chordwise pressure distributions at the 94 percent radius station were essentially unaffected by the tip shapes investigated. The largest differences in the pressure distributions were near the tip and toward the trailing edge, and were associated with the rearward sweep of the tip vortices over the upper surfaces of the blades. The extent of the affected surface areas was greater for the larger blade pitch angles in each case. However, for the same blade pitch angle, the affected surface area was smaller for the blade with the body-of-revolution tip since the path of its tip vortex was outboard of that of the blade with the square, flat tip.

For the blade with the square, flat tip and at the 99.5 percent radius, the suction pressure peak associated with the passage of the primary tip vortex was as large as the suction peak near the leading edge. At blade pitch angles of 6.18 degrees and 11.4 degrees, a secondary suction peak of lower magnitude was detected on the square-tipped blade and this was associated with the formation of a secondary vortex.

For the blade with the body-of-revolution tip, there were no suction peaks similar to those detected on the square-tipped blade. At the 91 percent chordwise pressure orifice, the suction pressure on the round-tipped blade was still increasing and, at the 99.5 percent radius, was approximately equal in magnitude to the value of the suction peak at the leading edge.

INTRODUCTION

The aerodynamic loadings on rotor blade tips and wing tips are highly influenced by the formation, growth, and subsequent passage of the tip vortex over their upper surfaces. Pressure measurements (references 1-5) obtained for wings operating at unstalled angles of attack show that the three-dimensional tip relief considerably reduces the magnitude of the suction pressure peak near the leading edge. The data also indicate the appearance of low pressure regions near the tip and aft of the maximum thickness position, and this phenomenon has been attributed to the formation, growth, and passage of the tip vortex (references 2 and 3). The magnitude of this second suction pressure peak may be as high or higher than that near the leading edge at the same span station. Very near the tip and closer to the trailing edge, a third suction peak of lower magnitude has been observed (references 3-5) and this has been attributed to the formation of a secondary tip vortex. As a result, instead of falling off uniformly to zero as the tip is approached, the wing section lift coefficient decreases and then increases to approximately 50-70 percent of its value at the midspan station (depending on the angle of attack). Thus, the lower pressures associated with the tip vortex on the upper surface aft of the maximum thickness maintain higher lift coefficients than would otherwise exist and this effect is favorable. However, there is a corresponding rearward shift in center of pressure, and this coupled with the higher lift coefficient results in significant increases in the section pitching moment in the nose-down direction and, approximately, a doubling of the pressure drag coefficient. These latter effects are unfavorable both from a performance and a structural design viewpoint.

Although this tip loading phenomenon has been known for over 60 years (reference 1), there was apparently little further work done in this area. It was recognized (reference 2) that the measured tip loadings deviated considerably from those predicted by the theoretical state-of-the-art at that time. However, until the advent of the high-speed digital computer, theories with empirical drag corrections formed an acceptable basis for design of higher aspect ratio wings for many years, since the tip loadings were a small part of the total loadings. For low aspect ratio and delta wings, other approaches had to be found and developed.

In the middle of the 1960's, experimental studies were begun on tip modifications to reduce helicopter rotor noise (reference 6) and to allieviate compressibility effects on the tip (reference 3). In reference 3, tip pressure measurements are presented for a yawed wing in a wind tunnel as a simulation of a rotor blade under forward flight conditions. These measured pressure distributions were similar to those of the earlier studies but, in addition, pointed out the existence of a secondary vortex formation outboard of the primary vortex. Reference 3 also reports the results of flow visualization studies near the tips of wings and hovering rotors, and concludes that the geometric configurations of the corresponding tip vortices with respect to their generating surfaces are essentially the same for low Mach numbers. Reference 7 presents pressure measurements obtained from an NACA 0012 airfoil-section rotating blade with a square, flat tip and compares the distributions with those for an NACA 0015 wing. These latter data are found in reference 5 but were obtained from the tests of reference 4. If the point of vortex inception is defined as that position along the chord where the pressure gradient changes sign, then it was found that, for the rotating blade, the primary vortex location was generally further aft and outboard than that for the fixed wing. Since the blade and wing had different airfoil sections, the question of what effect different operating environments have on tip vortex location was not completely resolved. The results of reference 7 were also compared with the flow visualization studies of reference 8 for a rotating blade. The location of the point of vortex inception was found to be about 5 percent ahead of that determined by flow visualization, but this may be subject to the interpretation involved in both cases.

The tip vortex/blade interference may be more important for the rotating blade than for wings of higher aspect ratio. This possibility arises from the fact that, for the blade, the phenomenon occurs in the area of the highest dynamic pressure. Also, the corresponding rearward shift in center of pressure may have significant effects on blade structural dynamics and design and on control system loads. In addition, the higher pressure drag that is associated with the tip vortex formation occurs at the greatest blade radius and the highest dynamic pressure, and this will affect the power required appreciably (reference 4).

One conclusion that can be reached from the above discussion is that the simple tip-loss factor (reference 9) and lifting-line/blade-element/prescribed-wake analyses (for example, references 10 and 11) are not satisfactory for computing the true tip effects for rotor blades. Recent studies on wings and rotors (for example, references 12-15) and NASA-supported studies (references 16 and 17, for example) have been directed at the development of a satisfactory analytical method. The principal problem appears to be the lack of a suitable model for the tip vortex shedding mechanism and the subsequent interaction with the blade surface as the vortex passes rearward. A related problem involves uncertainties concerning the applicability of semi-span wing data to rotor blades in hover.

The studies presented here were undertaken in an attempt to provide further insight into the problem of tip effect and to provide baseline data for validating the forthcoming theoretical and numerical analyses. The specific purpose of the tests to be described was to acquire and analyze, with respect to tip vortex formation, the pressure distribution on a hovering rotor blade having a body-of-revolution tip. Also, these data were compared with data that were acquired for the same blade with a square, flat tip.

SYMBOLS

D	rotor diameter, meters
c	blade chord length, meters
C_{p_r}	pressure coefficient, $(p - p_\infty)/q$
C_{p_R}	pressure coefficient based on tip speed
p	blade surface pressure, newtons per square meter
p_∞	atmospheric pressure, newtons per square meter
q	dynamic pressure, newtons per square meter, $\frac{1}{2}\rho\Omega^2 r^2$

r	blade radius station, meters
R	blade radius of square, flat tip and radius of attachment plane for half-body of revolution tip, meters
y	distance inboard from R, meters
θ	blade pitch angle, degrees
ρ	atmospheric density, kilograms per cubic meter
Ω	blade angular velocity, radians per second

APPARATUS AND PROCEDURE

Test Facility

The experiments were conducted in the helicopter rotor research facility at Georgia Tech, shown in figures 1 and 2a. The test cell is made of wood and has a barricade of steel and wood for a distance of 0.6 m on either side of the rotor plane. The interior dimensions are 2.74 x 2.74 x 6.40 m. The cell is partitioned by a honeycomb which suppresses the turbulence in the return flow. This honeycomb partition has a large circular hole centered on the axis of rotation of the rotor, and a bellmouth duct is installed in this hole to provide for a freer and more uniform passage of the rotor wake. Ventilation ports reduce the incidence and intensity of tornado-like vortices which were observed extending from the thrust side of the rotor to the walls of the cell.

Although the flow in the test cell is not completely smooth, the fluctuations are rather small. Measurements made near the rotor plane of the mean axial velocity distribution and tip vortex location and the measured rotor performance are in reasonable agreement with the results of a prescribed-vortex-wake analysis for an isolated rotor. This confirms that the rotor is operating in hover within the test cell with no appreciable wall effect.

The rotor is attached to the drive shaft with flexures which constitute a strain gage balance system. In this way, rotor thrust and torque can be measured if desired. The rotor is driven by a variable-speed motor rated at 11.2 kW.

Blade Tip Assembly

The model rotor blade has a constant chord of 12.7 cm and a tip radius of 61 cm, with an NACA 0012 untwisted section (fig. 2b). The outermost 4.45 cm is made of magnesium and is removable. This removable tip was made in two pieces, each 2.22 cm wide, which were cemented along the chordwise interface and held together by through-bolts. Additional bolts secured the tip to the rotor blade. Before the two pieces of the tip were cemented together, matching holes ranging in diameter from 5.16 mm to 1.59 mm were drilled into each piece from the mating surface side, and groups of these holes were joined together by slots milled in the mating surfaces so as to form six cavities (see fig. 3). The largest hole in each group was drilled through the inboard side of the assembly and tapped to receive a transducer mounting plug. Surface pressure orifices 0.64 mm in diameter were drilled from the airfoil surface into the six cavities. These orifices were located in chordwise planes at spanwise stations 94.0, 96.6, 98.0, 98.7, 99.1, and 99.5 percent of blade radius. In each plane, an orifice was located at the leading edge of the section, and 20 holes were located on both the upper and the lower surfaces.

The transducer plugs extended approximately 1.78 cm into the cavities, and each plug had a milled flat on which was cemented a paddle-type subminiature pressure transducer. The flats were perpendicular to the blade chordline in order that the transducers could be mounted so as to minimize inertial force effects. The two tip pieces were glued together. The tip then was bolted to the rotor blade and the transducer wires were led to the rotor hub.

The finished blade thus has a tip containing six irregularly-shaped cavities, with each cavity containing a pressure transducer which is exposed to pressure on the blade surface through the several orifices drilled into the cavity. A typical cavity is shown in figure 3b.

A round tip was constructed by turning a body of revolution from mahogony to an NACA 0012 contour and then milling away half of the body. When needed, this round tip was attached to the outboard surface of the flat tip by bolts.

Instrumentation

Surface pressures (gage) were measured using paddle-type pressure transducers. These transducers have an active 4-arm bridge bonded to a stainless steel diaphragm 3.18 mm in diameter. The nominal output of these gages is 0.15 μ v/N/m^2 per volt of excitation. The sensitivity of these gages to inertial loads tangential to the diaphragm surface is quoted as being 0.09 mv/1000 "g". The transducers are temperature compensated, but the change in air temperature in the rotor test chamber during the course of a test run was negligible.

The output of the transducers was conducted from the rotor hub through mercury sliprings to high quality DC amplifiers which were operated at a gain of 200. The signals were then routed through a scanner to an integrating digital voltmeter. Data acquisition was accomplished using a mini-computer.

If zero adjustment of the transducer bridge output is desired, the balancing circuit must be located prior to the slip rings, otherwise inaccuracies due to changes in slip ring resistance during a run are introduced. For simplicity, no zero adjustment was made. The small zero offset of the gages was not troublesome.

The rotor speed was determined by electronically counting the pulsed output of a magnetic pickup which sensed the passage of the teeth of a gear which was mounted on the drive shaft. The speed was held within $\pm$1 revolution per minute at any pre-selected value.

Procedure

Static Calibration. - The pressure transducers in the rotor tip were statically calibrated in place by applying known pressures to each cavity. This was accomplished by fitting an air-tight lucite box over the end of the rotor blade, the box being sealed at its inboard end with an O-ring around the blade contour. This box was pressurized with nitrogen, and the box pressure was read on an electronic manometer while the corresponding output of the pressure transducers was read with a digital voltmeter. Using 3 volts excitation, the gages in cavities 1-5 had outputs in the range of 0.32 - 0.42 μ v/N/m^2 (without amplification) while the gage in cavity 6 had an output of 0.19 μ v/N/m^2. The output of all six gages was linear with applied pressure and repeatable within 1.5 percent. This

static calibration procedure was performed periodically during the course of the tests, with excellent repeatability. The calibration factors derived in this calibration agreed almost exactly with those obtained for the same transducers some two years earlier, as reported in reference 7. The only exception was the transducer in cavity 4; it was found to behave erratically at the start of the present tests and was replaced.

Acceleration Corrections.- When diaphragm-type pressure transducers, such as those used here, are installed in an accelerating system such as a rotating blade, there is an inertial load on the gage which results in deflection of the diaphragm and the generation of an output signal which cannot be distinguished from that due to an applied pressure. This effect may be minimized by ensuring that the inertial load is parallel to the diaphragm. Accordingly, the gages in the tip were carefully installed so that the diaphragm surfaces were perpendicular to the blade chordline. This arrangement served to minimize the significant inertial load due to centripetal acceleration (1200 g's at the diaphragm radial station at 1350 RPM). Since the extended quarter-chord line of the blade intersected the rotor axis of rotation, there was a small component of this intertial load which acted perpendicular to the diaphragm, being smallest for the gage mounted nearest the blade pitch axis and largest for the gage nearest the trailing edge. This component changes slightly with blade pitch angle. There is also a small normal component of inertia loading, which varies with blade pitch angle, that is due to coning of the blade during rotation (the coning angle at maximum thrust was approximately 0.2 degrees). The acceleration corrections were experimentally determined at pitch angles of 0, 6.2, and 11.4 degrees, and the effect of pitch angle could not be distinguished (i.e. all of the data fell within the repeatability of the acceleration correction at zero degrees). Accordingly, a common "g" correction for each gage was applied at all pitch angles.

The acceleration correction for the transducers due to diaphragm inertial loading was found by first sealing all of the pressure orifices by covering the tip with plastic tape which was next covered with a layer of strippable plastic paint so as to minimize leaks. The blade then was run up to operating RPM. The resulting output of the gages was caused by the inertial loading on the diaphragm and also on the column of air trapped in each cavity. The effect of the inertia loading on the air column is to reduce the pressure (initially atmospheric pressure) at the transducer, and this correction was calculated for a given RPM so that the diaphragm inertial loading effect could be determined. Extreme care had to be taken in sealing the pressure orifices during these acceleration runs. The

free volume of the cavities is small, and a small leak into or out of this closed volume results in a significant change in pressure on the diaphragm. With proper sealing, the outputs of the transducers were essentially constant during acceleration evaluation runs. The "g" corrections were found to be in the range of 135-800 N/m^2 (depending upon the gage) and were repeatable within $\pm$ 50 N/m^2 or approximately 1 percent of the test dynamic pressure. The corrections as determined during these tests were in satisfactory agreement with those obtained earlier as reported in reference 7.

If, as was usually the case, the orifice exposed during pressure measurement is at a different radial location than the transducer diaphragm, there is a pressure gradient due to the "g" effects on the air column. This gradient was calculated and the data were corrected for this effect.

Data Acquisition. - The rotor tip was carefully covered with plastic tape, and one orifice into each cavity was opened by piercing the hole with a needle. The six transducer voltages were read, with the digital voltmeter set to integrate and average over 0.1 seconds, and were printed on a teletype. Before starting a test, readings were taken to establish the zero drift. An acceptable zero drift of the gage output was taken to be a change of less than 10 microvolts (which corresponded to about 25 N/m^2) in one minute. If the zero drift was acceptable, the rotor was brought up to the desired RPM in less than 15 seconds and the outputs of the six transducers were sampled and recorded over a time interval of 30 seconds. The rotor then was stopped in less than 10 seconds and zero readings were taken to ensure that an acceptable drift rate had been maintained. In general, the zero drift was not a problem. Values of gage pressure were calculated by subtracting the last initial zero reading from the first pressure measurement at speed and also by subtracting the last pressure reading at speed from the first zero readings taken after the rotor was stopped. These two differences were then averaged to comprise one gage-pressure data point.

Data for each pressure orifice were taken sequentially at the three different pitch angles by the method described above. The plastic tape was then removed, the blade was re-taped, and six other orifices were selected for measurement.

After correcting the data for acceleration effects, the data were expressed in pressure coefficient form by using the ambient air density and the local blade velocity (C_{p_r}) or the blade tip speed (C_{p_R}). From a consideration of the data acquisition and

analysis procedures, it is estimated that the pressure coefficients are accurate to within 1 percent of the dynamic pressure (a ΔC_p of approximately plus or minus 0.01).

RESULTS AND DISCUSSION

The surface pressure measurements were made at a Reynolds number of 736,000 and a Mach number of 0.25, both based on tip speed. Although these numbers are considerably smaller than those encountered in full-scale operation and the single-bladed rotor is rarely used in practice, the results presented here are applicable to the primary objective of the experiment. This was one of providing data to suggest and validate analytical methods for calculating tip pressure loadings on rotor blades and for comparison with semi-span model wing data for the same range of test conditions.

The data for the blade with the body-of-revolution tip are given in tables 1-3 and the data for the blade with the square, flat tip in tables 4-6. Each value in the tables is the average of all the data taken at a particular location and test condition. Because of the location of the attachment bolts, there were no pressure taps at the 10.5 and 21.5 percent chord locations for the inner three radial stations nor at the 11.5 and 18.5 percent chord locations for the outer three radial stations. The few gaps in the data for the 60.5, 65, and 69 percent chord stations indicate that these readings were not sufficiently repeatable to be reliable. The transducer used to measure the pressures at these locations proved to be erratic under the high centrifugal loading.

The values of pressure coefficient for the blade with the square, flat tip in tables 4-6 are new and are not simply a copy of the tables of reference 7, which present data taken with the same test apparatus several years earlier. There are generally only small differences in the values of pressure coefficient between the two sets of data for locations ahead of the 60.5 percent chord station, although the difference can be as large as 0.05 in C_p in a few places. However, the differences aft of this location are, in some cases, larger than 0.10 in C_p. The reason for this disagreement is not known. The data of reference 7 were repeatable and consistent when those data were acquired and the new data were equally repeatable and consistent. The question of whether to use the data of reference 7 or to repeat the measurements for the square, flat tip was resolved through a detailed consideration of the data for the blade pitch angle of 0 degrees as follows.

First, it was believed that there should be little difference in the pressure distributions for the blade with the body-of-revolution tip and the blade with the square, flat tip at the 94 percent radius station. This was verified by the new data. Second, the mean profile drag coefficient as determined from torque measurements for the blade with the square, flat tip was 0.0097. Integration of the original pressure distribution for the blade with the square, flat tip (reference 7) gave a section chordwise force coefficient (pressure drag) of approximately 0.014 which seemed much too high in comparison with the torque-derived value and with the two-dimensional value (reference 18) of 0.0067, since the actual profile drag coefficient which includes both pressure and skin friction drag should be higher than the chordwise force coefficient due only to pressure drag. Integration of the data presented herein for the blade with the square, flat tip gave a value for the chordwise force coefficient of 0.0046, which differs from the two-dimensional value by an amount which can be attributed to skin friction drag. Although this latter value of chordwise force coefficient is more reasonable, this does not completely validate the new data since some of the pressure data trends at angle of attack suggest that the true distribution may lie between the two sets of data (as presented here and in reference 7) for the square-tipped blade.

Thus, it was decided to repeat the measurements for the square, flat tip rather than to use the results of reference 7 as the reference case because it was felt that the comparison with the new body-of-revolution tip data would be more valid. The missing data in tables 4-6 near the leading edge for the square-tipped blade represent data points that were not taken in order to reduce the testing time.

Figure 4 compares the pressure distribution for the body-of-revolution tip at the 94 percent station and a blade pitch angle of 0 degrees with that from reference 19 and with the two-dimensional potential flow distribution from reference 20. The experimental data from reference 19 were obtained by traversing a pitot-static tube in the plane of symmetry of a rectangular wing which had an NACA 0012 airfoil section and an aspect ratio of 6. Since the rotor blade in hover is revolving in its own wake, the actual dynamic pressure will be less than that based on the blade angular velocity. The extrapolation to zero degrees of torque measurements made at small angles of collective pitch with this model rotor indicates a 10 percent smaller, approximately, dynamic pressure. Thus, the corrected rotor blade pressure coefficients would be higher than those shown and it would appear that the agreement would be quite good except toward the trailing edge, as would be expected.

Blade Pitch Angle Equal to 0 Degrees

Figures 5a through f compare the non-lifting pressure distributions (C_{p_r}) for the blade with a body-of-revolution tip with those for a square, flat tip. Figure 6 shows the same data presented as contours of constant pressure coefficient, C_{p_R}, where now all of the pressure coefficient values are based upon the same (tip) speed. The pressure coefficients plotted in Figures 5 and 6 are the average for the upper and lower blade surfaces.

Examination of these two figures indicates that at the innermost measurement station at 94 percent radius (fig. 5a) the pressure distributions for the two tips are identical within experimental error except over the forward 5 percent and the rearmost 25% of the chord. As one proceeds outboard from the 94% radius station, the addition of the body of revolution tip causes only a small change in the pressure distribution.

Blade Pitch Angle of 6.18 Degrees

Figures 7a through f compare the pressure distributions (C_{p_r}) for the blade with a body-of-revolution tip (table 2) with the one having a square, flat tip (table 5) at a blade pitch angle of 6.18 degrees. Figures 8a through c show the same data (expressed as C_{p_R}) in the form of contours of constant pressure for both the upper and lower blade surfaces.

Examination of figures 7 and 8a indicates that the pressures on the lower surface of the blade are relatively insensitive to the variations in the flow caused by the different tip shapes except very near the blade tip. However, the upper surface pressures are significantly affected by the change in tip shape.

The effects of the tip vortices on the pressure distributions are locally large on the upper surface. For the square-tipped blade, the effects associated with the passage of the tip vortex first begin to appear in the pressure distributions as a reversal in sign of the chordwise pressure gradient between the 84.4 and 91 percent chord stations at the 98 percent radius (fig. 7c). At the 98.7 percent radius (fig. 7d), the point of pressure-gradient sign reversal has moved forward to about the 77 percent chord station. At the 99.1 percent radius (fig. 7e), the point of pressure-gradient sign reversal has moved forward to the 56.5 percent chord station and a suction peak occurs at the 77 percent chord station. At the 99.5 percent radius (fig. 7f and table 5), the point of pressure-gradient sign reversal

has moved further forward to near the 40 percent chord station. At this outermost station, a suction peak of nearly the same magnitude as that near the leading edge occurs at the 60 percent chord station, and there is an indication of a secondary suction peak of much lower magnitude at the 84.4 percent chord station. These suction peaks are attributed to the close passage of a primary tip vortex and a secondary vortex over the upper surface of the blade (references 2 and 3) and, therefore, should be an indication of the radial and chordwise location of these vortices.

The presence of these suction peaks is indicated in figure 8b by a crowding together of the constant pressure contours. The primary vortex originates at the tip somewhat forward of mid-chord and then sweeps inboard and aft. In the preceding paragraph, the appearance of the secondary suction peak in the chordwise pressure distribution data was taken to indicate the presence of a secondary vortex. However, close examination of the surface pressure distributions during the construction of the constant pressure contours of figure 8b indicates that this conclusion cannot be drawn with certainty. The density of the pressure orifice coverage on the upper surface of the rotor tip outboard of the 99% radius and aft of 60% chord is not adequate to eliminate ambiguity in the construction of the pressure contours. An alternate interpretation of the existing data suggests that the secondary suction peak may be attributed to the presence of the primary vortex. However, since an equally good case for the presence of a secondary vortex can be made from the data, and since the secondary vortex has been noted by other investigators using flow visualization at wing tips (reference 2 and 3), the secondary vortex is the interpretation chosen here.

For the blade with the body-of-revolution tip, a comparison of the pressure coefficient distributions at the 98 and 98.7 percent radius (figs. 7c and d) indicates a slight decrease in the pressure on the upper surface near the trailing edge at the 98.7 percent radius. At the 99.1 percent radius (fig. 7e), there is a definite reversal of the sign of the chordwise pressure gradient at the 77 percent chord station, and again this is attributed to the passage of the tip vortex over the upper surface. At the 99.5 percent radius (fig. 7f), the point of sign reversal in the pressure gradient has moved forward to the 65 percent chord station. Unlike the square-tipped blade, the data for the round-tipped blade do not indicate a suction peak within the chordwise extent in which pressures were measured. However, the pressures must reach a minimum near the trailing edge before increasing to

satisfy the trailing edge condition of no pressure discontinuity with that of the lower surface. The presence of the tip vortex is also apparent in the pressure contours of figure 8c.

The above discussion regarding sign reversal and the presence of suction peaks may be summarized in the following table.

$\theta = 6.18^{o}$ Upper Surface	r/R (%) / Tip Shape	98.0	98.7	99.1	99.5
Location of sign reversal (% chord)	Square	84.4 - 91	77	56.5	40
	Round	None	None	77	65
Location of suction peaks (% chord)	Square	2.0 only	2.0 only	2.0, 77	2.0,60,84.4
	Round	2.0 only	2.0 only	2.0,> 91	2.0 > 91

There is, then, a large difference between the pressure distributions on the upper surface for the blade with the round tip and those for the square-tipped blade. The added body-of-revolution tip forces the tip vortex to form further outboard (as referenced to the radius, R) than in the case of the square, flat tip. As a consequence, the tip vortex of the round-tipped blade has a much smaller influence on the pressure distribution than does the tip vortex of the square-tipped blade. Although these differences in pressure distribution can significantly affect the local section lift and drag coefficients, it is not clear what the overall effect on performance would be, since the pressure distributions were not measured on the revolved surface of the body-of-revolution tip (i.e. for $r/R > 1.0$).

Blade Pitch Angle of 11.4 Degrees

Figures 9a through f compare the pressure distributions (C_{p_r}) for the blade with a body of revolution tip (table 3) with those for a square, flat tip (table 6) at a blade pitch angle of 11.4 degrees. Figures 10a through c show the same data as contours of constant pressure, C_{p_R}.

Inspection of figures 9 and 10a indicates that, as in the case of the blade pitch angle of 6.18 degrees, there is little effect on the pressure levels on the lower surface when the tip shape is changed.

The effects of the tip vortices on the pressure distributions are locally large on the upper surface (fig. 9 and figs. 10b and c). The locations of the sign reversal in the chordwise pressure gradient and the character of the chordwise pressure distributions aft of the leading edge suction peak are greatly altered, as can be seen from the following table, which is constructed from examination of figure 9.

$\theta = 11.4^{\circ}$ Upper Surface	r/R (%) / Tip Shape	98.0	98.7	99.1	99.5
Location of sign reversal (% chord)	Square	77	42	32	27
	Round	None	None	52	42
Location of suction peaks (% chord)	Square	1.5 only	1.5, 84	1.5, 62	2.0, 42, 69
	Round	1.5 only	1.5 only	1.5, > 91	1.0,> 91

The presence of the strong suction pressure peak aft of the leading edge suction peak on the upper surface of the blade with the square, flat tip is also apparent in the crowding of the constant pressure contours in figure 10b. This suction peak is again attributed to the close passage of a primary tip vortex over the upper surface of the blade (references 2 and 3). The most rearward suction peak at 99.5% radius is thought to be due to the formation and rearward movement of a secondary vortex. However, as was the case at a blade pitch angle of 6.18 degrees, the number of pressure taps available in this region precludes a firm conclusion in this regard. A comparison of figures 8b and 10b for the two different pitch angles shows that a larger area of the upper surface of the blade is affected by the tip vortex at a blade pitch angle of 11.4 degrees, and the line of suction pressure peaks has moved inboard and forward for this higher blade-pitch-angle case.

For the blade with the body-of-revolution tip, the above table, together with a comparison of figures 10b and 10c, indicates a large difference between the pressure distributions on the upper surface of this blade and the blade with the square, flat tip. The added body-of-revolution tip forces the tip vortex to form further outboard (as referenced to the radius, R) than in the case of the square flat tip, and the suction peak associated with this vortex is downstream of the last chordwise measurement station (i.e. > 91% chord). A comparison of figures 8c and 10c shows that, as in the case of the square, flat tip, the tip vortex from the body-of-revolution tip affects the upper surface pressures over a larger region as the blade pitch angle is increased.

It is again emphasized that, although these differences in pressure distribution with tip shape can significantly affect the local lift and drag coefficients, it is not clear what the overall effect on performance would be at a blade pitch angle of 11.4 degrees since pressure distributions were not measured on the revolved surface of the body-of-revolution tip for $r/R > 1.0$.

CONCLUSIONS

Blade-tip surface pressure measurements were made on a single-bladed, hovering helicopter rotor with two tip shapes. The rotor had a constant-chord, untwisted blade with a square, flat tip and the pressue distributions on this blade were compared with those measured on the same blade with a half-body of revolution tip. The data were obtained for each blade at six spanwise stations covering the 94 to the 99.5 percent radius at blade collective pitch angles of 0, 6.18, and 11.4 degrees. The Reynolds number based on tip speed and blade chord was 736,000 and the tip Mach number was 0.25. Based on the measured pressure distributions, the following major conclusions are reached for the two tip shapes at the given test conditions.

1. For the square, flat tip, the presence of the primary tip vortex causes the pressure distribution on the upper surface of the rotor very near the tip to exhibit an additional suction peak aft of the leading edge peak. This strong extra peak occurs at both $\theta = 6.18$ degrees and $\theta = 11.4$ degrees. The pressure distribution for the round-tipped blade does not define such a suction peak, at least within the region where data were taken. In this latter case, the pressures associated with the tip

vortex passage are still decreasing at the 99.5% blade radius and 91% chord station, the rearmost point where there was a pressure orifice.

2. The area of the upper surface of the rotor blades over which the pressures are significantly changed by the presence of the tip vortex is largest for the square, flat tip at θ = 11.4 degrees. If the sign reversal in the chordwise pressure gradient is used to define the surface area affected by the passage of the tip vortex, this area is roughly triangular in shape and outboard of a line extending from approximately 28% chord at r/R = 0.995 to 72% chord at r/R = 0.98.

3. The area of the upper surface over which the pressures are significantly changed by the presence of the tip vortex is smaller for the body-of-revolution tip both at θ = 6.18 degrees and θ = 11.4 degrees because the effect of the round tip is to cause the tip vortex to form further outboard as referenced to the radius, R.

4. On the upper surface of the blade with the square, flat tip, the strong suction peak due to the primary tip vortex is nearly equal in magnitude to that of the leading edge suction peak at θ = 6.18 degrees and is 70%-80% of the magnitude of the leading edge suction peak at θ = 11.4 degrees. With the round tipped blade, the pressure coefficient at 99.5% radius at the 91% chord station is about one-half the magnitude of the leading edge suction peak at the same radius at θ = 6.18 degrees and about 80% of the magnitude of the leading edge suction peak at the same radius at θ = 11.4 degrees.

5. For both tips, the effect of increasing blade pitch angle is to move the tip vortex inboard on the upper surface and to cause it to grow stronger. Thus, the tip vortex moves inboard with increased loading, but the tip vortex of the round-tipped blade remains outboard relative to the tip vortex of the square-tipped blade.

6. For the square, flat tip the data suggest that there is a weaker secondary tip vortex on the upper surface which is outboard and aft of the primary tip vortex at both θ = 6.18 degrees and θ = 11.4 degrees. The pressure distribution measured on the round-tipped blade does not indicate any such secondary tip vortex for the range of test conditions investigated.

7. On the lower surface of the blade, the effect on the pressure distribution due to the different tip shapes is minor inboard of approximately 98% blade radius at both θ = 6.18 degrees and θ = 11.4 degrees.

8. At 0 degrees pitch angle, the two different blade tips produce small but measurable differences in the surface pressure distribution near the tip.

9. At the 94% radius, there are only minor differences in the surface pressure distribution for the two blade tips at the same collective pitch angle.

REFERENCES

1. Munk, Max: Die Druckverteilung uber Tragflachen nach englischen Messungen. Z. Flugtech. Motorluftschiffahrt, Jahrgang VII, Heft 19 u. 20, Okt. 28, 1916, pp. 133-137.

2. Knight, Montgomery; and Loeser, Oscar, Jr.,: Pressure Distribution over a Rectangular Monoplane Wing Model up to 90° Angle of Attack. NACA TR 288, 1928.

3. Spivey, Richard F.: Blade Tip Aerodynamics - Profile and Planform Effects. Preprint 205, 24th Annual Nat. Forum, Am. Helicopter Soc., (Washington, D.C.), May 1968.

4. Spivey, W. A.; and Morehouse, G. G.: New Insights into the Design of Swept-Tip Rotor Blades. Preprint 420, 26th Annual Nat. Forum, Am. Helicopter Soc., (Washington, D. C.), June 1970.

5. Chigier, N. A.; and Corsiglia, V. R.; Tip Vortices - Velocity Distributions. Preprint 522, 27th Annual Nat. Forum, Am. Helicopter Soc., (Washington, D. C.), May 1971.

6. Spencer, R. H.; Sternfield, H., Jr.; and McCormick, B. W.: Tip Vortex Core Thickening for Application to Helicopter Rotor Noise Reduction. U. S. Army, USAAVLABS TR 66-1, Sept. 1966.

7. Shivananda, T. P.; McMahon, H. M.; and Gray, R. B.: Surface Pressure Measurements at the Tip of a Model Helicopter Rotor in Hover. J. Aircraft, vol. 15, no. 8, August, 1978, pp. 460-467.

8. Hoffman, J. D.; and Velkoff, H. R.: Vortex Flow over Helicopter Rotor Tips. J. Aircraft, vol. 8, no. 9, Sept. 1971, pp. 739-740.

9. Wheatley, John B.: An Aerodynamic Analysis of the Autogiro Rotor with a Comparison between Calculated and Experimental Results. NACA TR 487, 1934.

10. Gray, Robin B.: An Aerodynamic Analysis of a Single-Bladed Rotor in Hover and in Low-Speed Forward Flight as Determined from Smoke Studies of the Vorticity Distribution in the Wake. Ph.D. Thesis, Princeton University, 1957. (Also Princeton U. Aero. Eng. Dept. Rep. 356, 1956).

11. Landgrebe, Anton J.: An Analytical and Experimental Investigation of Helicopter Rotor Hover Performance and Wake Geometry Characteristics. U. S. Army, USAAMRDL TR 71-24, June 1971.

12. Sopher, Robert: Three-Dimensional Potential Flow Past the Surface of a Rotor Blade. Preprint 324, 25th Annual Nat. Forum, Am. Helicopter Soc., (Washington, D. C.), May 1969.

13. Kocurek, J. David; and Tangler, James L.: A Prescribed Wake Lifting Surface Hover Performance Analysis. J. Am. Helicopter Soc., vol. 22, no. 1, Jan. 1977, pp. 24-35.

14. Raj, Pradeep; and Gray, Robin B.: Computation of Three-Dimensional Potential Flow Using Surface Vorticity Distribution. J. Aircraft, vol. 16, no. 3, Mar. 1979, pp. 162-169.

15. Shenoy, K. Rajarama: A Method of Computing the Pressure Distribution on a Single-Bladed Hovering Helicopter Rotor. Ph.D. Thesis, Georgia Institute of Technology, 1979.

16. Hall, G. F.; Shamroth, S. J.; McDonald, H.; and Briley, W. R.: The Invisid Pressure Field on the Tip of a Semi-Infinite Wing and Its Application to the Formation of a Tip Vortex. NASA CR-2748, 1976.

17. Shamroth, S.J.; and Briley, W.R.: A Viscous Flow Analysis for the Tip Vortex Generation Process. NASA CR 3184, 1979.

18. Jacobs, Eastman N.; and Sherman, Albert: Airfoil Section Characteristics as Affected by Variations of the Reynolds Number, NACA TR 586, 1937.

19. Silverstein, Abe; and Becker, John V.: Determination of Boundary-Layer Transition on Three Symmetrical Airfoils in the N.A.C.A. Full-Scale Tunnel. NACA TR 637, 1938.

20. Abbott, Ira H.; von Doenhoff, Albert E.; and Stivers, Louis S., Jr.: Summary of Airfoil Data. NACA TR 824, 1945.

Table 1

Pressure coefficient distribution based on local dynamic pressure.
Half-body of revolution tip on blade at 0 degrees pitch angle.

$\frac{r}{R} \times 100$	94.0	96.6	98.0	98.7	99.1	99.5
$\frac{1}{2}\rho\Omega^2 r^2$	4021 N/m^2	4247 N/m^2	4371 N/m^2	4434 N/m^2	4470 N/m^2	4506 N/m^2
% CHORD						
0.0	0.938	0.929	0.967	0.944	0.924	0.916
1.0	0.124	0.092	0.105	0.124	0.135	0.075
2.0	-0.134	-0.087	-0.123	-0.119	-0.146	-0.143
5.0	-0.338	-0.333	-0.295	-0.299	-0.294	-0.276
7.5	-0.367	-0.356	-0.335	-0.317	-0.311	-0.290
10.5				-0.322	-0.319	-0.302
11.5	-0.389	-0.366	-0.347			
18.5	-0.369	-0.350	-0.327			
21.5				-0.303	-0.289	-0.283
22.5	-0.359	-0.343	-0.312	-0.296	-0.288	-0.279
27.5	-0.330	-0.305	-0.282	-0.259	-0.264	-0.240
32.5	-0.298	-0.267	-0.246	-0.227	-0.221	-0.211
37.5	-0.278	-0.253	-0.228	-0.216	-0.209	-0.196
42.5	-0.252	-0.226	-0.209	-0.200	-0.195	-0.176
47.5	-0.230	-0.203	-0.194	-0.176	-0.171	-0.154
52.5	-0.203	-0.182	-0.167	-0.157	-0.148	-0.134
56.5	-0.179	-0.157	-0.137	-0.128	-0.133	-0.121
60.5	-0.153	-0.140	-0.146	-0.125	-0.130	-0.123
65.0	-0.142	-0.138	-0.104	-0.113	-0.120	-0.112
69.0	-0.117	-0.117	-0.106	-0.101	-0.109	-0.098
77.0	-0.087	-0.039	-0.047	-0.050	-0.065	-0.082
84.4	-0.044	-0.025	-0.021	-0.032	-0.037	-0.048
91.0	0.013	0.008	-0.001	-0.015	-0.021	-0.025

Table 2

Pressure coefficient distribution based on local dynamic pressure.
Half-body of revolution tip on blade at 6.18 degrees pitch angle.

$\frac{r}{R} \times 100$	94.0		96.6		98.0		98.7		99.1		99.5	
$\frac{1}{2}\rho\Omega^2 r^2$	4021 N/m^2		4247 N/m^2		4371 N/m^2		4434 N/m^2		4470 N/m^2		4506 N/m^2	
% CHORD	UPPER SURFACE	LOWER SURFACE	UPPER SURFACE	LOWER SURFACE	UPPER SURFACE	LOWER SURFACE	UPPER SURFACE	LOWER SURFACE	UPPER SURFACE	LOWER SURFACE	UPPER SURFACE	LOWER SURFACE
0.0	0.840	0.840	0.829	0.829	0.858	0.858	0.882	0.882	0.893	0.893	0.895	0.895
1.0	-0.749	0.685	-0.657	0.651	-0.617	0.618	-0.550	0.646	-0.467	0.582	-0.556	0.557
2.0	-0.920	0.436	-0.738	0.436	-0.782	0.412	-0.679	0.366	-0.646	0.304	-0.593	0.283
5.0	-0.808	0.068	-0.741	0.074	-0.681	0.054	-0.642	0.051	-0.600	0.026	-0.561	0.023
7.5	-0.760	-0.026	-0.701	-0.046	-0.638	-0.043	-0.590	-0.042	-0.566	-0.048	-0.521	-0.053
10.5							-0.542	-0.098	-0.514	-0.114	-0.480	-0.115
11.5	-0.691	-0.115	-0.616	-0.118	-0.567	-0.126						
18.5	-0.569	-0.163	-0.508	-0.188	-0.462	-0.186						
21.5							-0.411	-0.184	-0.387	-0.175	-0.378	-0.177
22.5	-0.519	-0.213	-0.486	-0.198	-0.430	-0.183	-0.405	-0.183	-0.391	-0.182	-0.359	-0.189
27.5	-0.455	-0.195	-0.415	-0.199	-0.362	-0.190	-0.332	-0.185	-0.317	-0.192	-0.295	-0.173
32.5	-0.396	-0.188	-0.307	-0.191	-0.274	-0.179	-0.263	-0.176	-0.261	-0.176	-0.256	-0.167
37.5	-0.326	-0.201	-0.266	-0.182	-0.250	-0.175	-0.247	-0.169	-0.249	-0.165	-0.243	-0.158
42.5	-0.280	-0.180	-0.252	-0.169	-0.230	-0.161	-0.222	-0.159	-0.222	-0.159	-0.219	-0.153
47.5	-0.269	-0.164	-0.202	-0.154	-0.196	-0.151	-0.198	-0.146	-0.203	-0.144	-0.210	-0.138
52.5	-0.213	-0.153	-0.178	-0.140	-0.176	-0.139	-0.177	-0.136	-0.203	-0.137	-0.186	-0.131
56.5	-0.188	-0.145	-0.169	-0.133	-0.161	-0.129	-0.166	-0.128	-0.180	-0.129	-0.184	-0.123
60.5	-0.184	-0.140	-0.163	-0.127	-0.155	-0.122	-0.159	-0.134	-0.173	-0.128	-0.188	-0.135
65.0	-0.166	-0.138	-0.151	-0.123	-0.144	-0.117	-0.151	-0.156	-0.148	-0.128	-0.182	-0.122
69.0	-0.123	-0.127	-0.128	-0.125	-0.102	-0.089	-0.169	-0.129	-0.170	-0.128	-0.221	-0.113
77.0	-0.106	-0.080	-0.059	-0.059	-0.073	-0.063	-0.087	-0.070	-0.140	-0.070	-0.274	-0.070
84.4	-0.046	-0.060	-0.024	-0.038	-0.045	-0.046	-0.082	-0.051	-0.195	-0.042	-0.300	-0.052
91.0	0.003	-0.021	-0.012	-0.023	-0.023	-0.023	-0.073	-0.037	-0.208	-0.030	-0.318	-0.028

Table 3

Pressure coefficient distribution based on local dynamic pressure.
Half-body of revolution tip on blade at 11.4 degrees pitch angle.

$\frac{R}{R}$ x 100	94.0		96.6		98.0		98.7		99.1		99.5	
$\frac{1}{2}\rho\Omega^2 r^2$	4021 N/m^2		4247 N/m^2		4371 N/m^2		4434 N/m^2		4470 N/m^2		4506 N/m^2	
% CHORD	UPPER SURFACE	LOWER SURFACE	UPPER SURFACE	LOWER SURFACE	UPPER SURFACE	LOWER SURFACE	UPPER SURFACE	LOWER SURFACE	UPPER SURFACE	LOWER SURFACE	UPPER SURFACE	LOWER SURFACE
0.0	0.265	0.265	0.373	0.373	0.425	0.425	0.511	0.511	0.579	0.579	0.637	0.637
1.0	-1.703	0.912	-1.472	0.883	-1.380	0.864	-1.224	0.863	-1.078	0.810	-1.152	0.783
2.0	-1.744	0.772	-1.441	0.738	-1.408	0.711	-1.209	0.649	-1.139	0.578	-1.036	0.543
5.0	-1.309	0.377	-1.115	0.351	-1.060	0.319	-0.978	0.315	-0.919	0.257	-0.852	0.239
7.5	-1.183	0.259	-1.063	0.208	-0.927	0.185	-0.852	0.166	-0.798	0.149	-0.758	0.126
10.5							-0.735	0.080	-0.706	0.048	-0.643	0.032
11.5	-0.927	0.117	-0.820	0.084	-0.725	0.045						
18.5	-0.691	-0.010	-0.590	-0.030	-0.530	-0.050						
21.5							-0.486	-0.079	-0.466	-0.089	-0.470	-0.093
22.5	-0.617	-0.057	-0.549	-0.065	-0.492	-0.075	-0.467	-0.078	-0.457	-0.098	-0.440	-0.094
27.5	-0.525	-0.067	-0.452	-0.095	-0.388	-0.100	-0.371	-0.104	-0.368	-0.113	-0.370	-0.117
32.5	-0.462	-0.083	-0.370	-0.101	-0.342	-0.104	-0.318	-0.110	-0.325	-0.119	-0.325	-0.120
37.5	-0.394	-0.122	-0.346	-0.105	-0.311	-0.114	-0.310	-0.118	-0.309	-0.122	-0.310	-0.124
42.5	-0.336	-0.101	-0.304	-0.106	-0.282	-0.112	-0.274	-0.115	-0.281	-0.127	-0.294	-0.128
47.5	-0.309	-0.101	-0.251	-0.100	-0.246	-0.111	-0.248	-0.112	-0.268	-0.119	-0.298	-0.122
52.5	-0.250	-0.096	-0.245	-0.094	-0.220	-0.104	-0.235	-0.110	-0.277	-0.118	-0.293	-0.124
56.5	-0.221	-0.092	-0.215	-0.096	-0.207	-0.101	-0.217	-0.105	-0.260	-0.115	-0.320	-0.120
60.5	-0.212	-0.100	-0.218	-0.084	-0.215	-0.113	-0.214	-0.115	-0.276	-0.117	-0.399	-0.130
65.0	-0.199	-0.110	-0.188	-0.078	-0.198	-0.106	-0.212	-0.107	-0.283	-0.120	-0.410	-0.130
69.0	-0.173	-0.096	-0.163		-0.199	-0.099	-0.213	-0.100	-0.309	-0.102	-0.446	-0.125
77.0	-0.112	-0.060	-0.089	-0.035	-0.133	-0.047	-0.187	-0.054	-0.456	-0.069	-0.612	-0.092
84.4	-0.060	-0.039	-0.062	-0.019	-0.080	-0.031	-0.171	-0.045	-0.681	-0.053	-0.763	-0.070
91.0	-0.029	-0.012	-0.046	-0.006	-0.057	-0.034	-0.153	-0.043	-0.694	-0.051	-0.953	-0.049

Table 4

Pressure coefficient distribution based on local dynamic pressure.
Square, flat tip on blade at 0 degrees pitch angle.

$\frac{r}{R} \times 100$	94.0	96.6	98.0	98.7	99.1	99.5
$\frac{1}{2}\rho\Omega^2 r^2$	4021 N/m^2	4247 N/m^2	4371 N/m^2	4434 N/m^2	4470 N/m^2	4506 N/m^2
% CHORD						
0.0	0.897	0.891	0.875	0.861	0.867	0.809
1.0	0.157	0.092	0.060	0.083	0.054	0.051
2.0	-0.104	-0.106	-0.140	-0.159	-0.179	-0.193
5.0	-0.295	-0.299	-0.288	-0.292	-0.291	-0.304
7.5	-0.368	-0.351	-0.340		-0.305	-0.305
10.5				-0.313	-0.304	-0.292
11.5	-0.384	-0.368	-0.338			
18.5	-0.362	-0.337	-0.305			
21.5				-0.267	-0.250	-0.219
22.5	-0.358	-0.325	-0.289	-0.263	-0.249	-0.220
27.5	-0.321	-0.295	-0.266	-0.233	-0.229	-0.191
32.5	-0.309	-0.256	-0.223	-0.206	-0.194	-0.170
37.5	-0.282	-0.238	-0.211	-0.193	-0.186	-0.163
42.5	-0.247	-0.220	-0.200	-0.188	-0.161	-0.148
47.5	-0.227	-0.204	-0.191	-0.161	-0.159	-0.139
52.5	-0.206	-0.174	-0.159	-0.140	-0.143	-0.141
56.5	-0.172	-0.160	-0.138	-0.128	-0.124	-0.143
60.5	-0.178	-0.160	-0.123	-0.121	-0.118	-0.145
65.0	-0.156	-0.119	-0.113	-0.130	-0.122	-0.126
69.0	-0.118	-0.105	-0.115	-0.110	-0.120	-0.115
77.0	-0.048	-0.028	-0.033	-0.041	-0.061	-0.107
84.4	-0.012	-0.004	-0.008	-0.021	-0.055	-0.101
91.0	0.028	0.023	-0.003	-0.006	-0.049	-0.094

Table 5

Pressure coefficient distribution based on local dynamic pressure.
Square, flat tip on blade at 6.18 degrees pitch angle.

$\frac{r}{R} \times 100$	94.0		96.6		98.0		98.7		99.1		99.5	
$\frac{1}{2}\rho\Omega^2 r^2$	4021 N/m^2		4247 N/m^2		4372 N/m^2		4434 N/m^2		4470 N/m^2		4506 N/m^2	
% CHORD	UPPER SURFACE	LOWER SURFACE	UPPER SURFACE	LOWER SURFACE	UPPER SURFACE	LOWER SURFACE	UPPER SURFACE	LOWER SURFACE	UPPER SURFACE	LOWER SURFACE	UPPER SURFACE	LOWER SURFACE
0.0	0.807	0.807	0.812	0.812	0.836	0.836	0.835	0.835	0.868	0.868	0.849	0.849
1.0	-0.686	0.671	-0.661	0.655	-0.611	0.590	-0.513	0.564	-0.493	0.500	-0.437	0.458
2.0	-0.931	0.441	-0.766	0.405	-0.755	0.368	-0.657	0.302	-0.627	0.237	-0.574	0.176
5.0	-0.806	0.072	-0.715	0.029	-0.639	-0.014	-0.607	-0.010	-0.559	-0.038	-0.498	-0.054
7.5	-0.752	-0.064	-0.680	-0.088	-0.613	-0.097	-0.560	-0.098	-0.513	-0.104	-0.464	-0.133
10.5							-0.499	-0.116	-0.452	-0.138	-0.408	-0.175
11.5	-0.679	-0.128	-0.611	-0.126	-0.540	-0.134						
18.5	-0.550	-0.179	-0.494	-0.181	-0.432	-0.176						
21.5							-0.386	-0.169	-0.340	-0.172	-0.304	-0.159
22.5	-0.516	-0.176	-0.461	-0.186	-0.387	-0.175	-0.341	-0.167	-0.346	-0.169	-0.296	-0.164
27.5	-0.455	-0.190	-0.396	-0.191	-0.351	-0.178	-0.296	-0.167	-0.277	-0.166	-0.262	-0.150
32.5	-0.382	-0.189	-0.312	-0.187	-0.278	-0.163	-0.264	-0.160	-0.247	-0.159	-0.243	-0.142
37.5	-0.337	-0.186	-0.280	-0.172	-0.264	-0.160	-0.250	-0.145	-0.257	-0.137	-0.250	-0.133
42.5	-0.285	-0.176	-0.268	-0.157	-0.265	-0.143	-0.234	-0.146	-0.252	-0.129	-0.291	-0.127
47.5	-0.254	-0.166	-0.236	-0.152	-0.229	-0.140	-0.233	-0.134	-0.243	-0.134	-0.388	-0.115
52.5	-0.235	-0.151	-0.216	-0.140	-0.213	-0.131	-0.225	-0.120	-0.263	-0.114	-0.486	-0.110
56.5	-0.202	-0.142	-0.209	-0.136	-0.217	-0.122	-0.197	-0.120	-0.252	-0.112	-0.500	-0.109
60.5	-0.222	-0.132	-0.195	-0.126	-0.198	-0.117	-0.214	-0.122	-0.347	-0.113	-0.524	-0.114
65.0	-0.211	-0.158	-0.166	-0.128	-0.181	-0.123	-0.206	-0.111	-0.361	-0.101	-0.516	
69.0	-0.145	-0.096	-0.153	-0.113	-0.191	-0.110	-0.198	-0.104	-0.430		-0.477	-0.073
77.0	-0.078	-0.055	-0.065	-0.045	-0.090	-0.035	-0.214	-0.039	-0.444	-0.041	-0.347	-0.042
84.4	-0.036	-0.023	-0.031	-0.023	-0.057	-0.016	-0.258	-0.029	-0.403	-0.015	-0.354	-0.018
91.0	0.013	0.034	-0.011	0.000	-0.080	-0.005	-0.296	-0.015	-0.409	-0.010	-0.369	-0.011

Table 6

Pressure coefficient distribution based on local dynamic pressure.
Square, flat tip on blade at 11.4 degrees pitch angle.

$\frac{r}{R} \times 100$	94.0		96.6		98.0		98.7		99.1		99.5	
$\frac{1}{2}\rho\Omega^2 r^2$	4021 N/m^2		4247 N/m^2		4371 N/m^2		4434 N/m^2		4470 N/m^2		4506 N/m^2	
% CHORD	UPPER SURFACE	LOWER SURFACE	UPPER SURFACE	LOWER SURFACE	UPPER SURFACE	LOWER SURFACE	UPPER SURFACE	LOWER SURFACE	UPPER SURFACE	LOWER SURFACE	UPPER SURFACE	LOWER SURFACE
0.0					0.108	0.108	0.514	0.514	0.619	0.619	0.641	0.641
1.0	-1.691	0.923	-1.467	0.909	-1.328	0.836	-1.136	0.811	-1.049	0.748	-0.871	0.654
2.0	-1.763	0.758	-1.436	0.709	-1.339	0.635	-1.137	0.584	-1.058	0.496	-0.920	0.409
5.0	-1.274	0.381							-0.804		-0.722	0.136
7.5	-1.013				-0.758		-0.796		-0.720		-0.636	
10.5							-0.673	0.040	-0.613	-0.004	-0.505	
11.5	-0.902	0.113	-0.804	0.068	-0.688	0.034						
18.5	-0.673	0.004	-0.566	-0.030	-0.507	-0.062						
21.5							-0.465	-0.088	-0.439	-0.105	-0.406	-0.118
22.5	-0.631	-0.031	-0.547	-0.062	-0.484	-0.091	-0.443	-0.083	-0.452	-0.102	-0.431	-0.133
27.5	-0.525	-0.062	-0.455	-0.091	-0.431	-0.099	-0.380	-0.100	-0.397	-0.111	-0.434	-0.123
32.5	-0.460	-0.076	-0.396	-0.097	-0.368	-0.097	-0.360	-0.107	-0.373	-0.120	-0.400	-0.124
37.5	-0.420	-0.092	-0.360	-0.097	-0.348	-0.112	-0.354	-0.102		-0.105	-0.624	-0.127
42.5	-0.358	-0.094	-0.338	-0.096	-0.344	-0.097	-0.326	-0.114	-0.434	-0.105	-0.744	-0.122
47.5	-0.317	-0.099	-0.306	-0.096	-0.314	-0.100	-0.343	-0.103	-0.513	-0.122	-0.716	-0.112
52.5	-0.290	-0.093	-0.279	-0.096	-0.293	-0.101	-0.357	-0.096	-0.631	-0.100	-0.648	-0.114
56.5	-0.251	-0.090	-0.269	-0.094	-0.290	-0.094	-0.392	-0.098	-0.705	-0.098	-0.575	-0.118
60.5	-0.236	-0.056	-0.260	-0.097	-0.295	-0.094	-0.457	-0.084	-0.719	-0.114	-0.584	-0.113
65.0	-0.236	-0.078	-0.241	-0.096	-0.283	-0.098	-0.479	-0.094	-0.728	-0.108	-0.604	-0.127
69.0	-0.197		-0.199	-0.087	-0.309	-0.098	-0.617	-0.093	-0.695	-0.095	-0.625	-0.114
77.0	-0.107	-0.022	-0.128	-0.004	-0.283	-0.013	-0.619	-0.021	-0.668	-0.024	-0.556	-0.049
84.4	-0.066	0.008	-0.113	-0.003	-0.363	-0.003	-0.715	0.001	-0.572	-0.009	-0.522	-0.028
91.0	-0.017	0.034	-0.094	0.006	-0.395	0.015	-0.645	-0.015	-0.510	-0.007	-0.404	-0.020

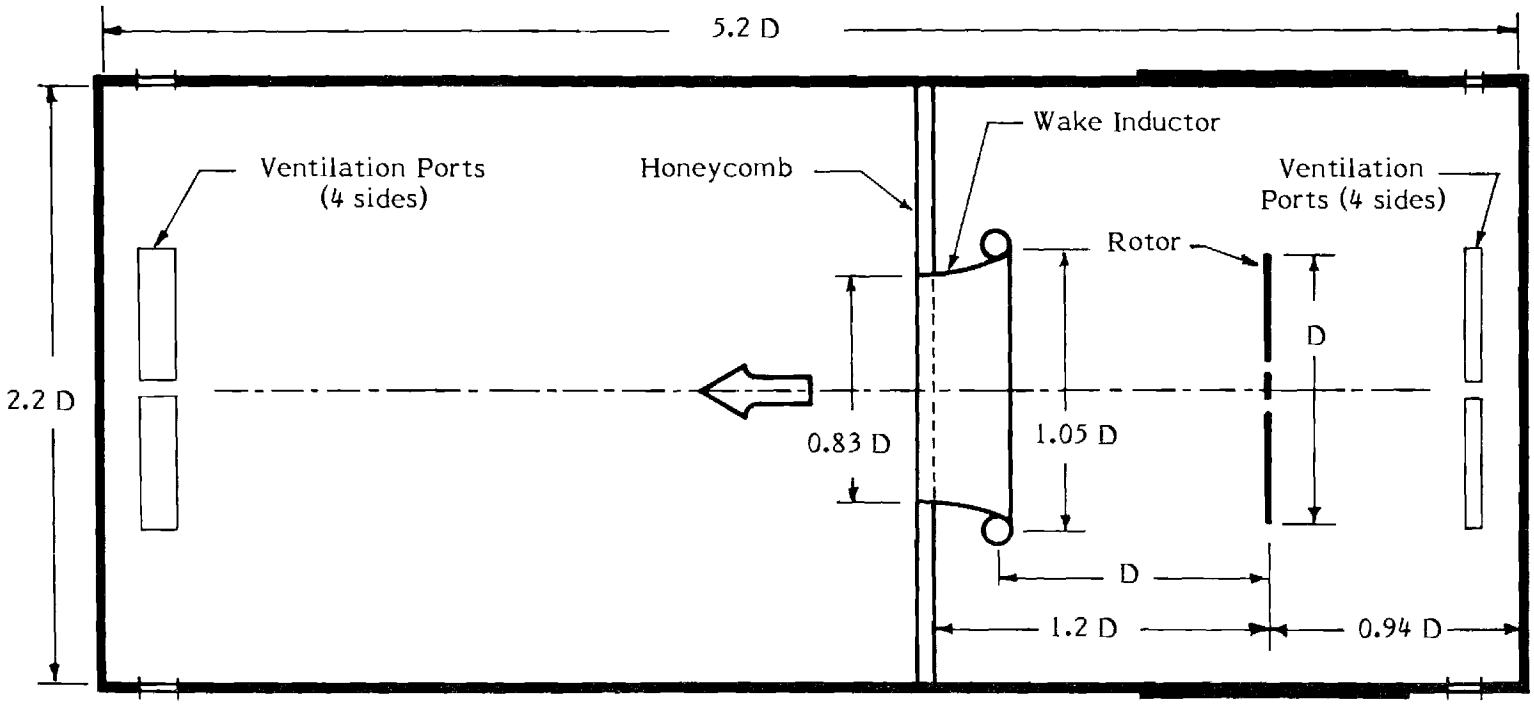

Figure 1. - Helicopter rotor test facility.

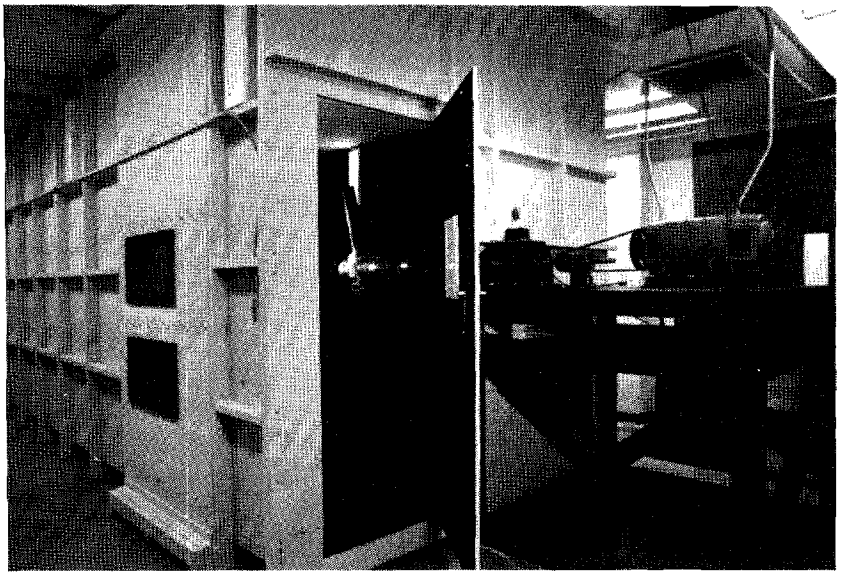

(a) Test facility.

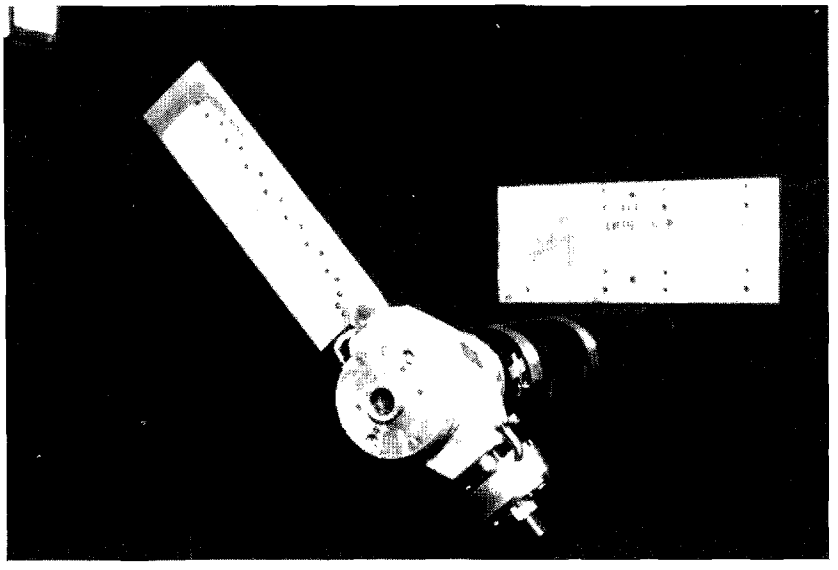

(b) Rotor blade.

Figure 2. - Photographs of test facility and rotor blade.

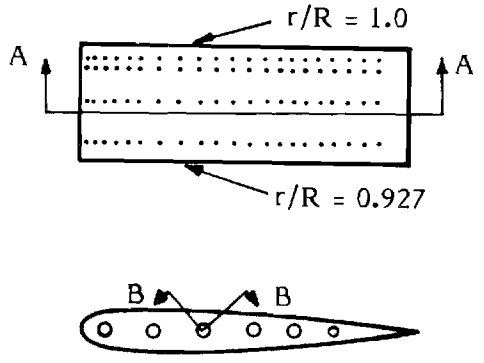

(a) Removable blade tip

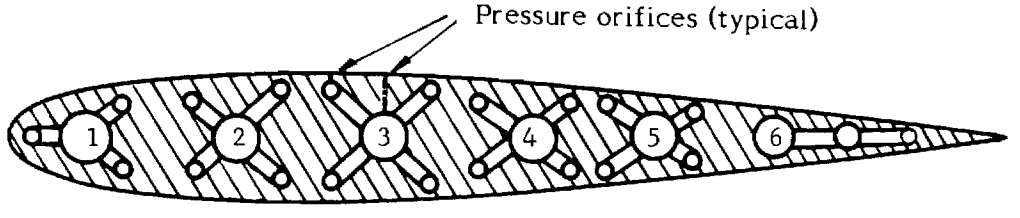

A-A

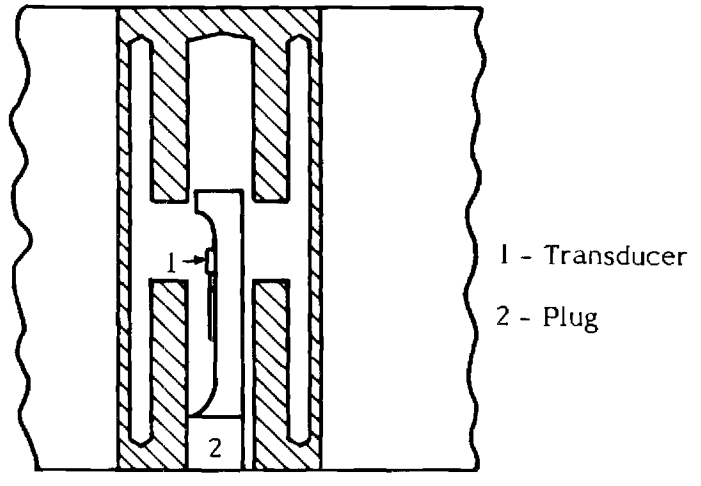

B-B

(b) Cross-sections

Figure 3. - Details of pressure tip design.

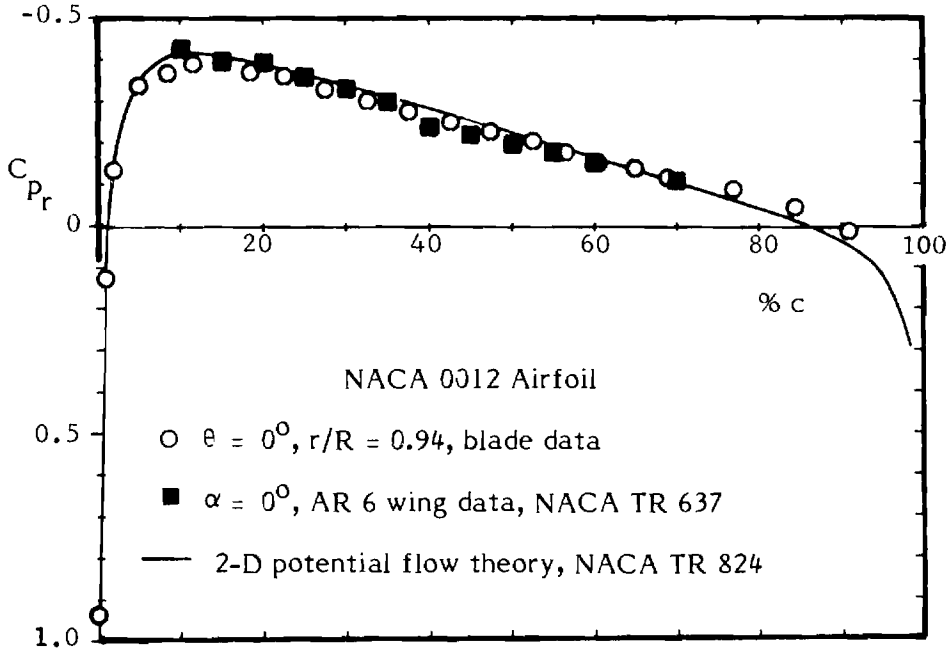

Figure 4. - Chordwise pressure coefficient data measured on a rotating blade compared with measured data on a wing of aspect ratio 6 and with two-dimensional potential flow theory results.

o Body of revolution tip

● Square, flat tip

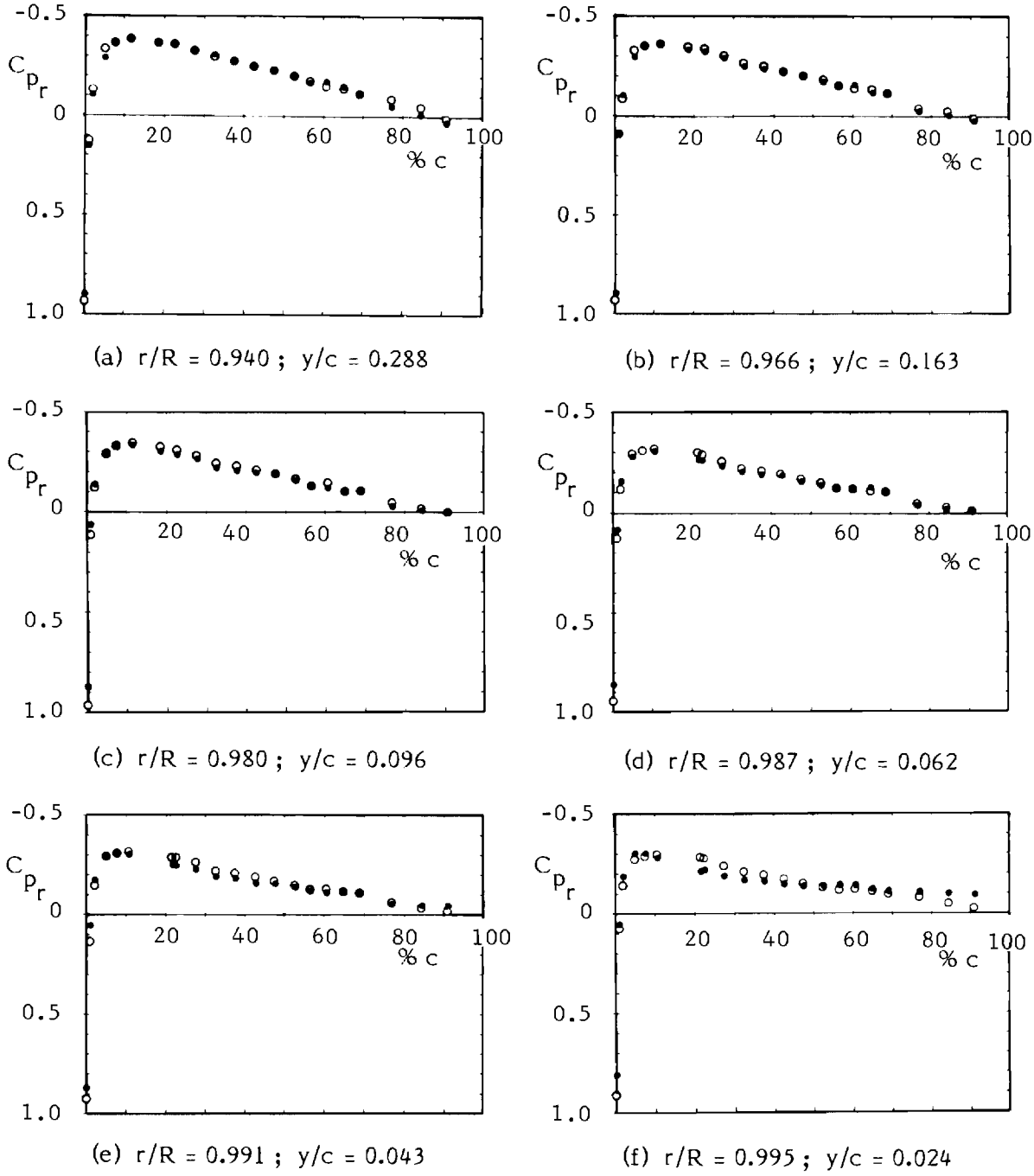

(a) r/R = 0.940 ; y/c = 0.288

(b) r/R = 0.966 ; y/c = 0.163

(c) r/R = 0.980 ; y/c = 0.096

(d) r/R = 0.987 ; y/c = 0.062

(e) r/R = 0.991 ; y/c = 0.043

(f) r/R = 0.995 ; y/c = 0.024

Figure 5. - Blade pitch angle of 0 degrees. Comparison of the pressure coefficient distribution based on local dynamic pressure and measured on a blade with a square, flat tip to the distribution on the same blade with a half-body of revolution tip.

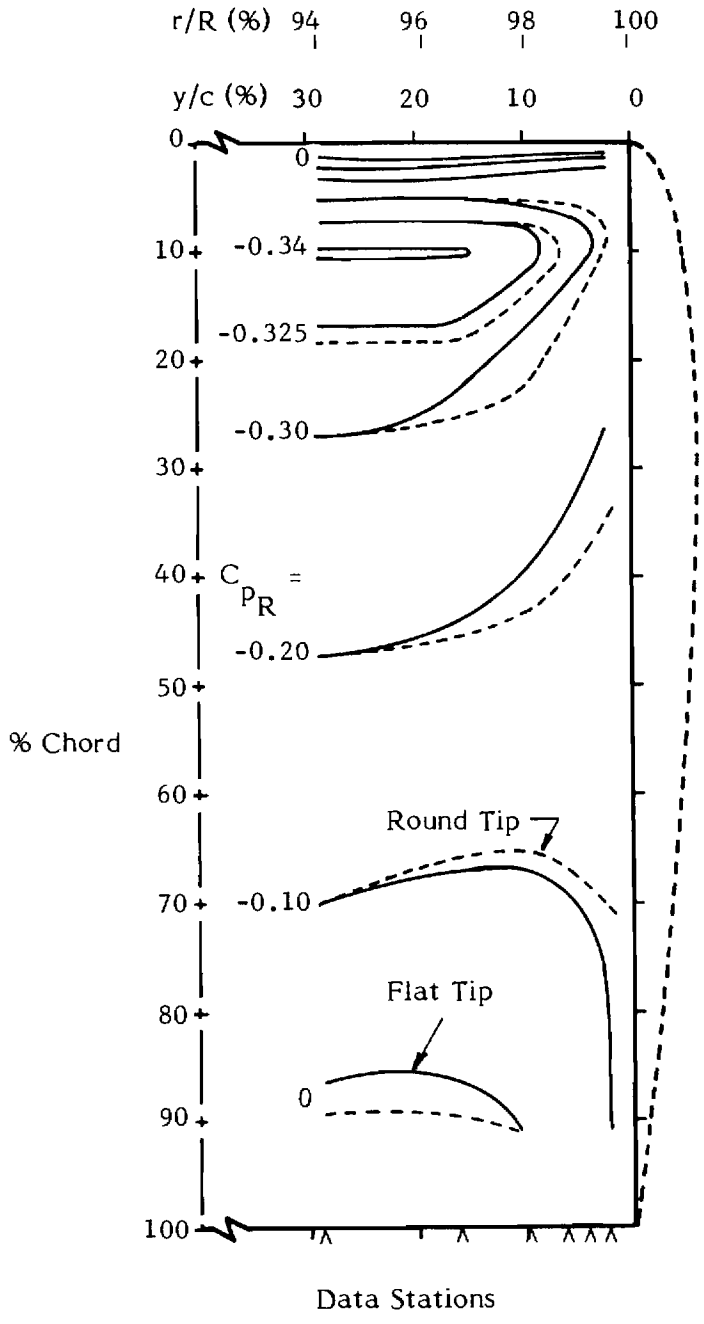

Figure 6. - Blade pitch angle of 0 degrees. Comparison of contours of constant pressure coefficient based on tip speed as measured on a blade with a square, flat tip and on the same blade with a half-body of revolution tip.

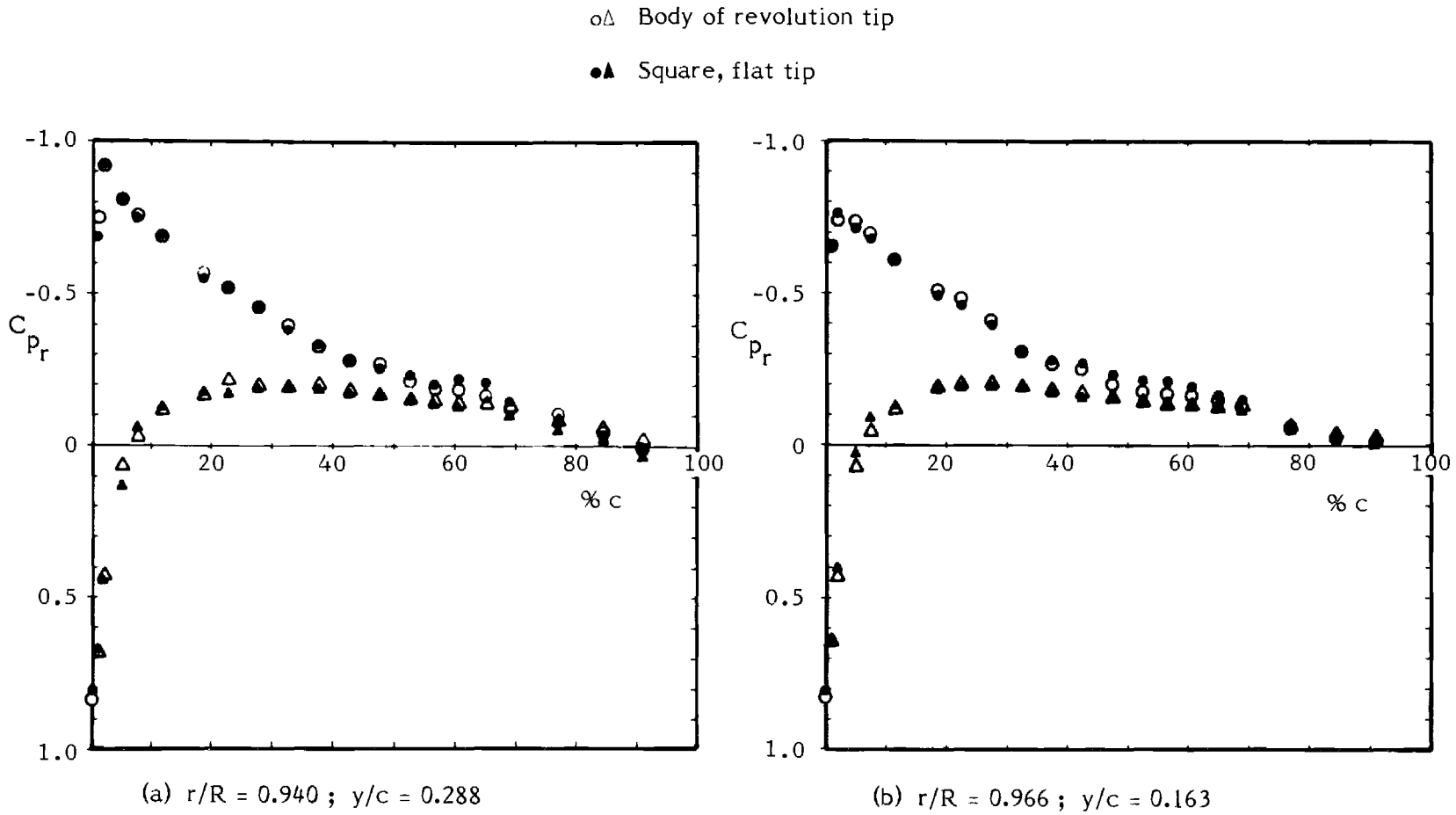

Figure 7. - Blade pitch angle of 6.18 degrees. Comparison of the pressure coefficient distribution based on local dynamic pressure and measured on a blade with a square, flat tip to the distribution on the same blade with a half-body of revolution tip.

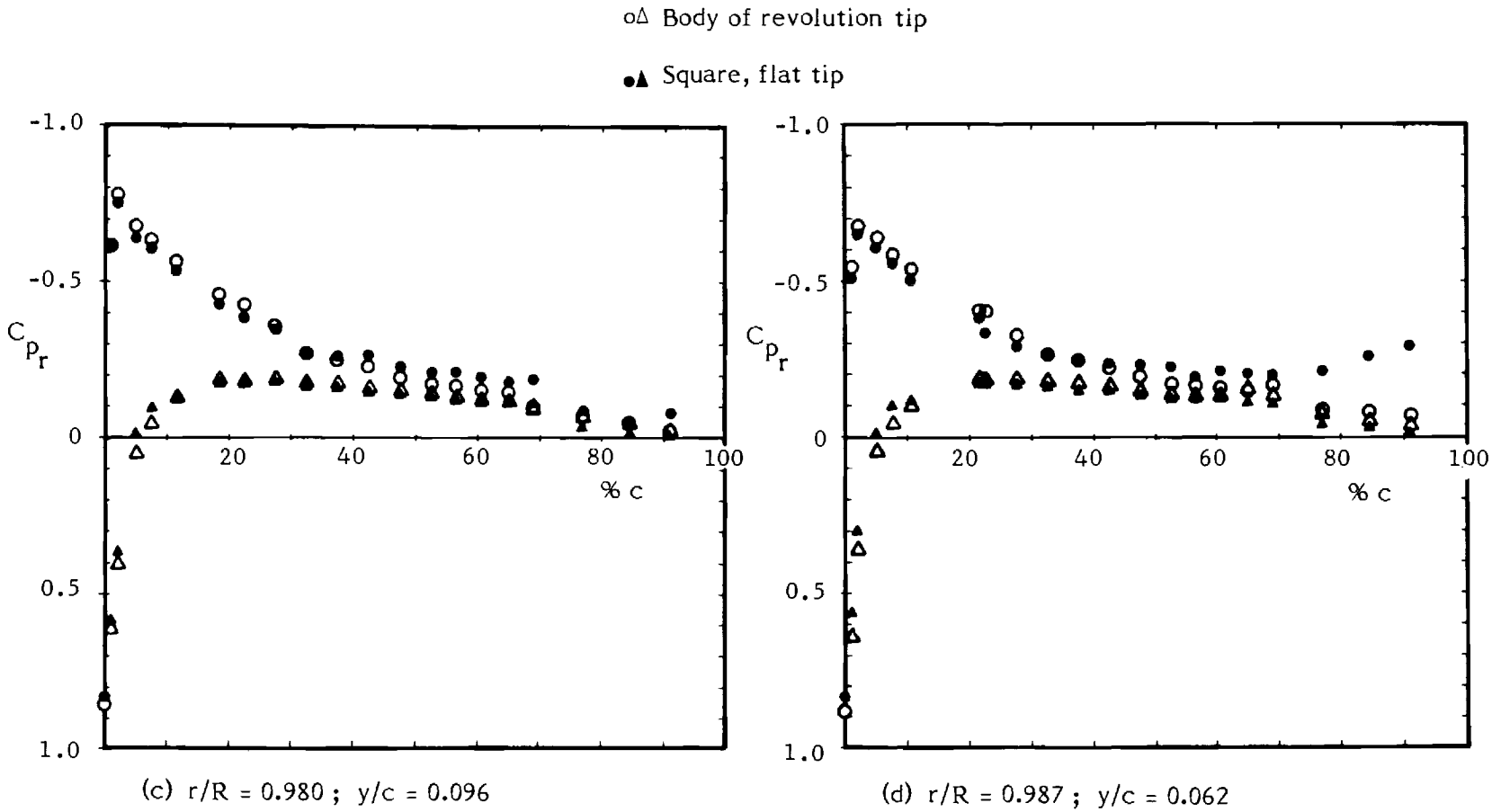

Figure 7. - (Continued)

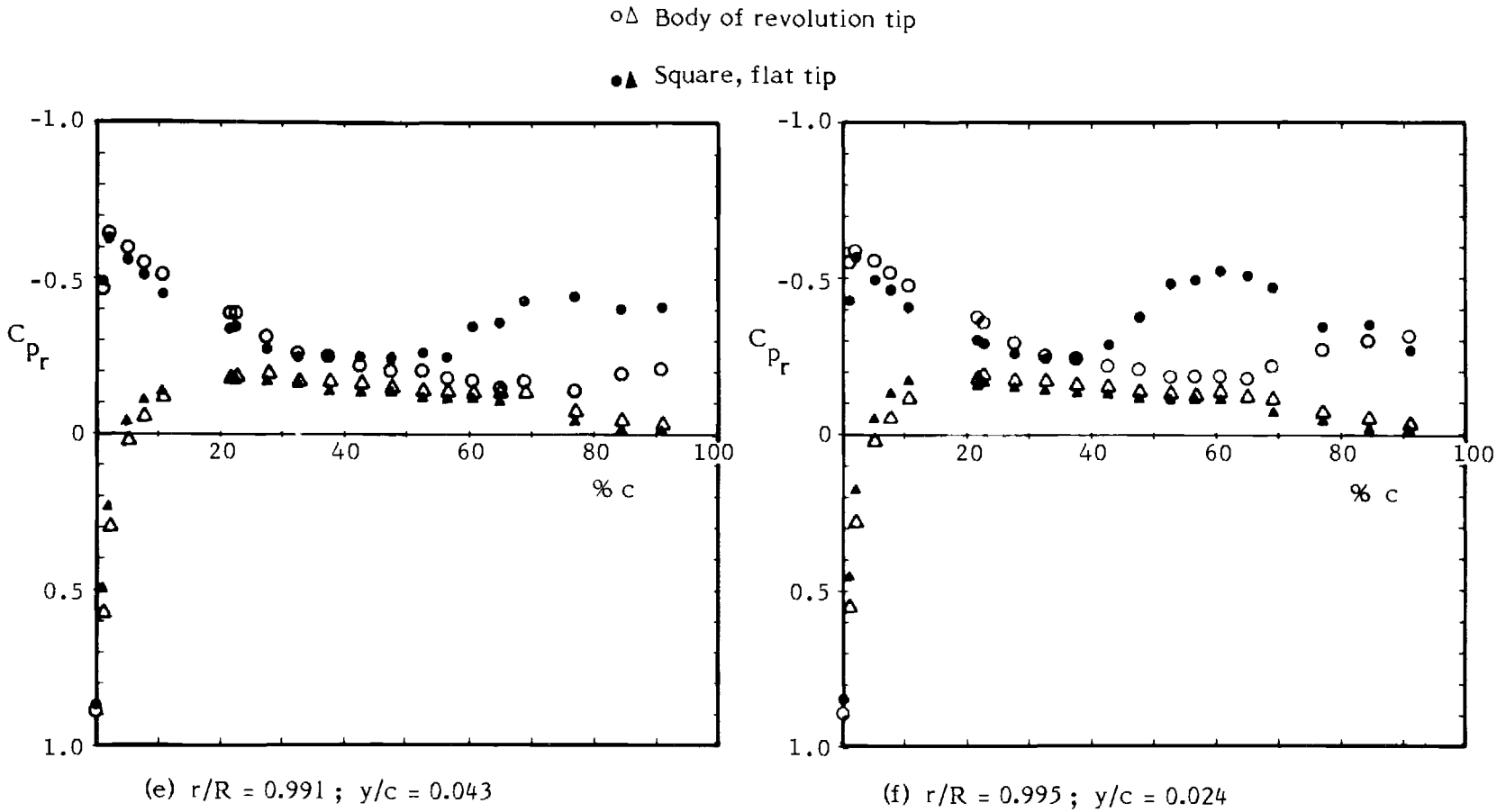

Figure 7. - (Concluded)

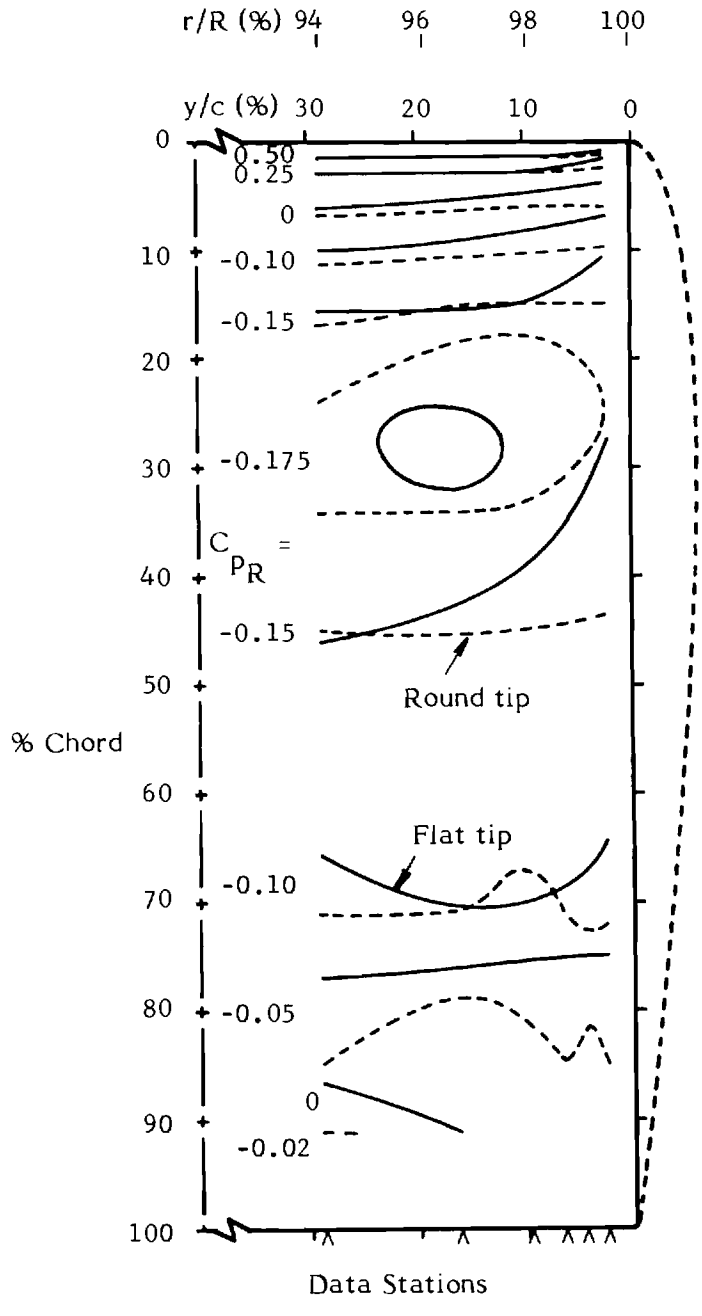

(a) Lower surface

Figure 8. - Blade pitch angle of 6.18 degrees. Comparison of contours of constant pressure coefficient based on tip speed as measured on a blade with a square, flat tip and on the same blade with a half-body of revolution tip.

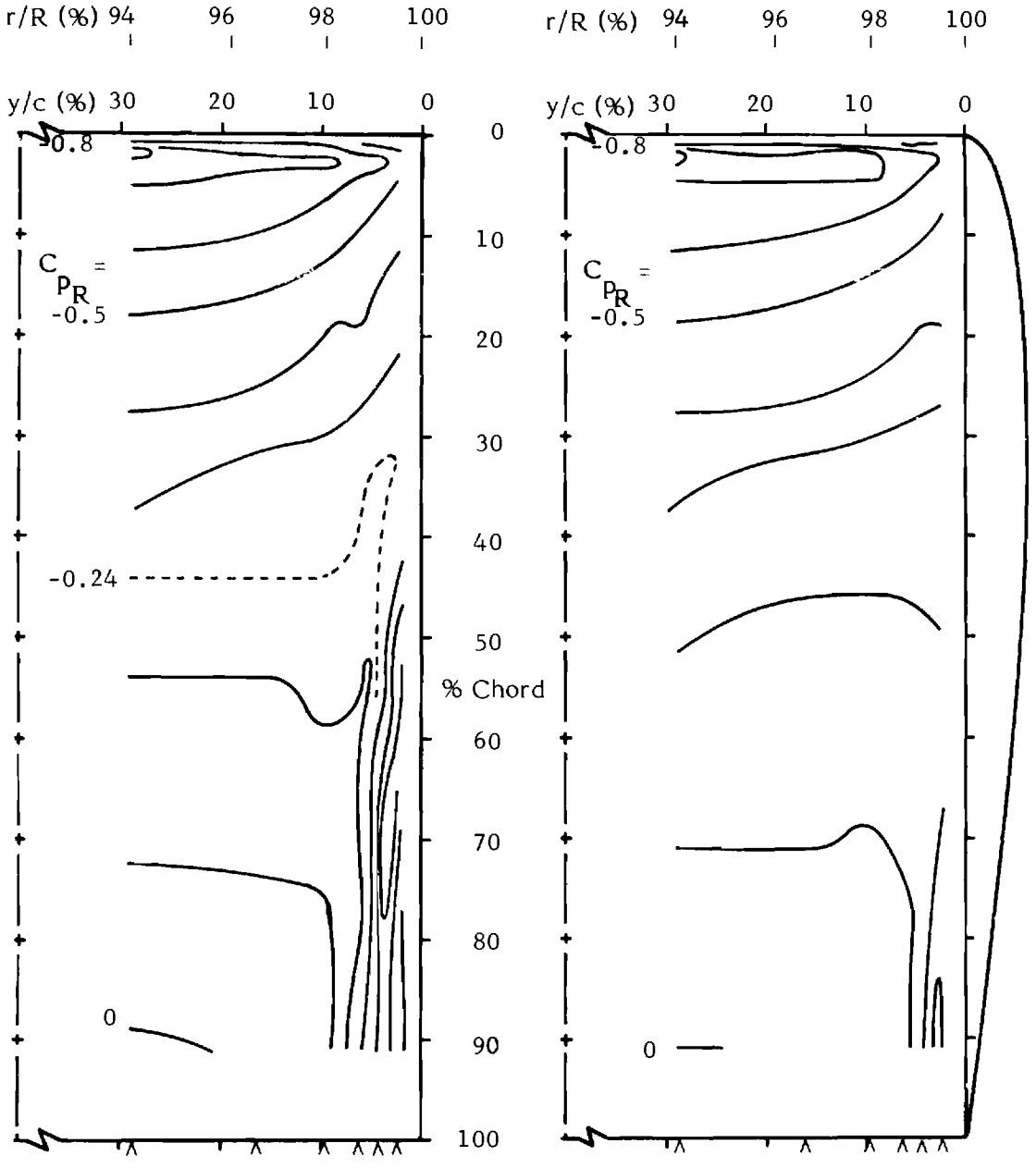

(b) Upper surface, flat tip

(c) Upper surface, round tip

Figure 8. - (Concluded)

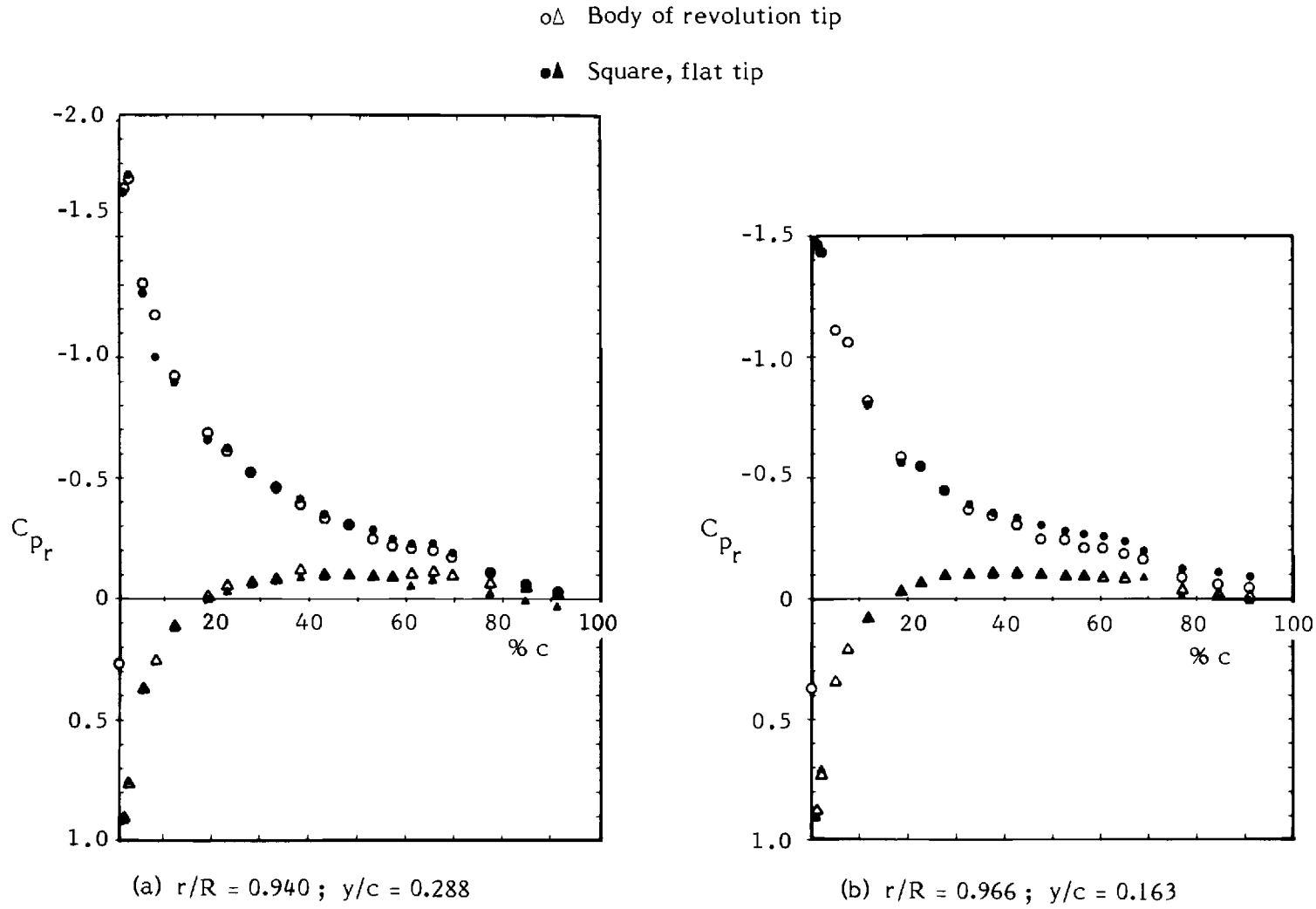

Figure 9. - Blade pitch angle of 11.4 degrees. Comparison of the pressure coefficient distribution based on local dynamic pressure and measured on a blade with a square, flat tip to the distribution on the same blade with a half-body of revolution tip.

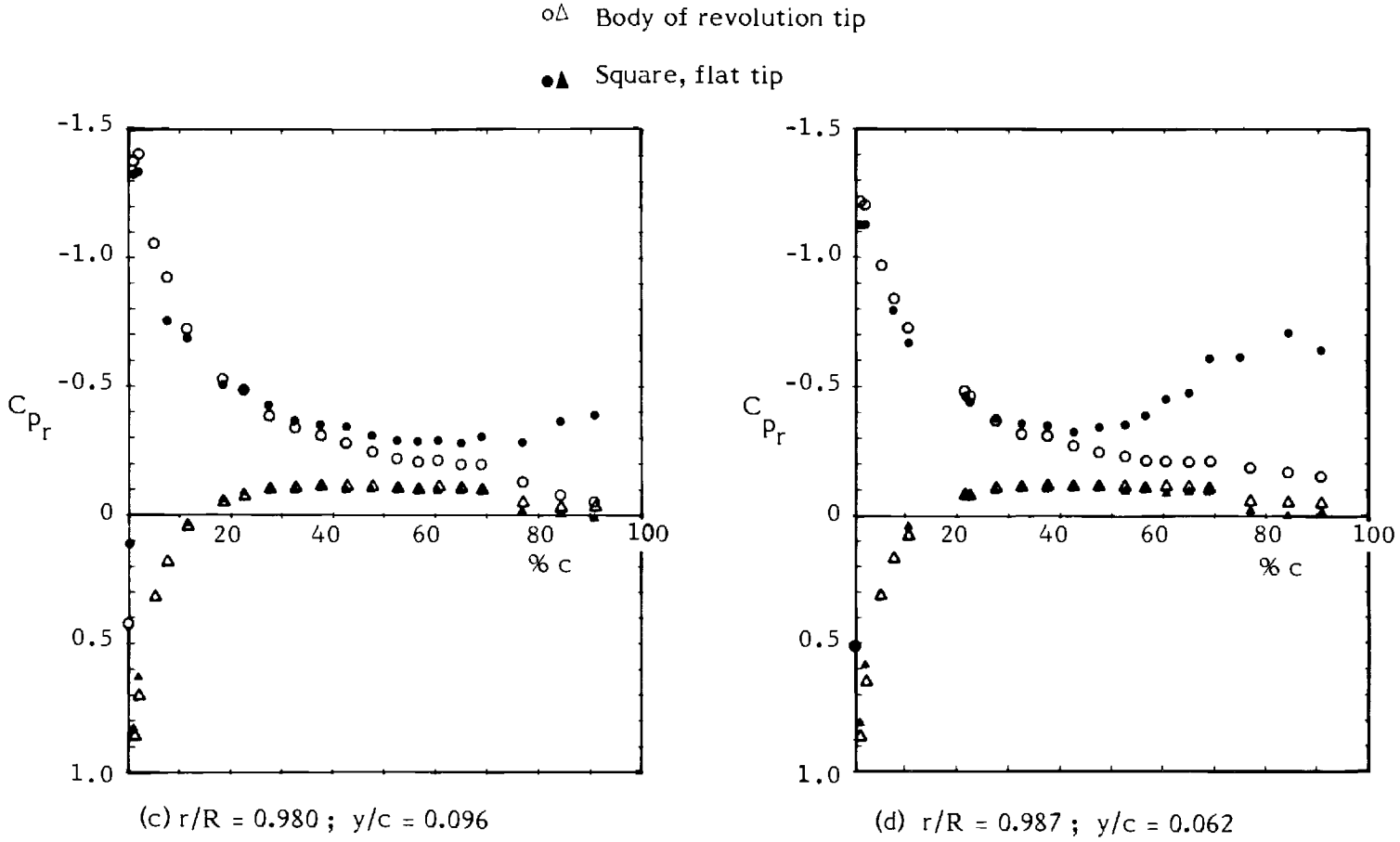

Figure 9. - (Continued)

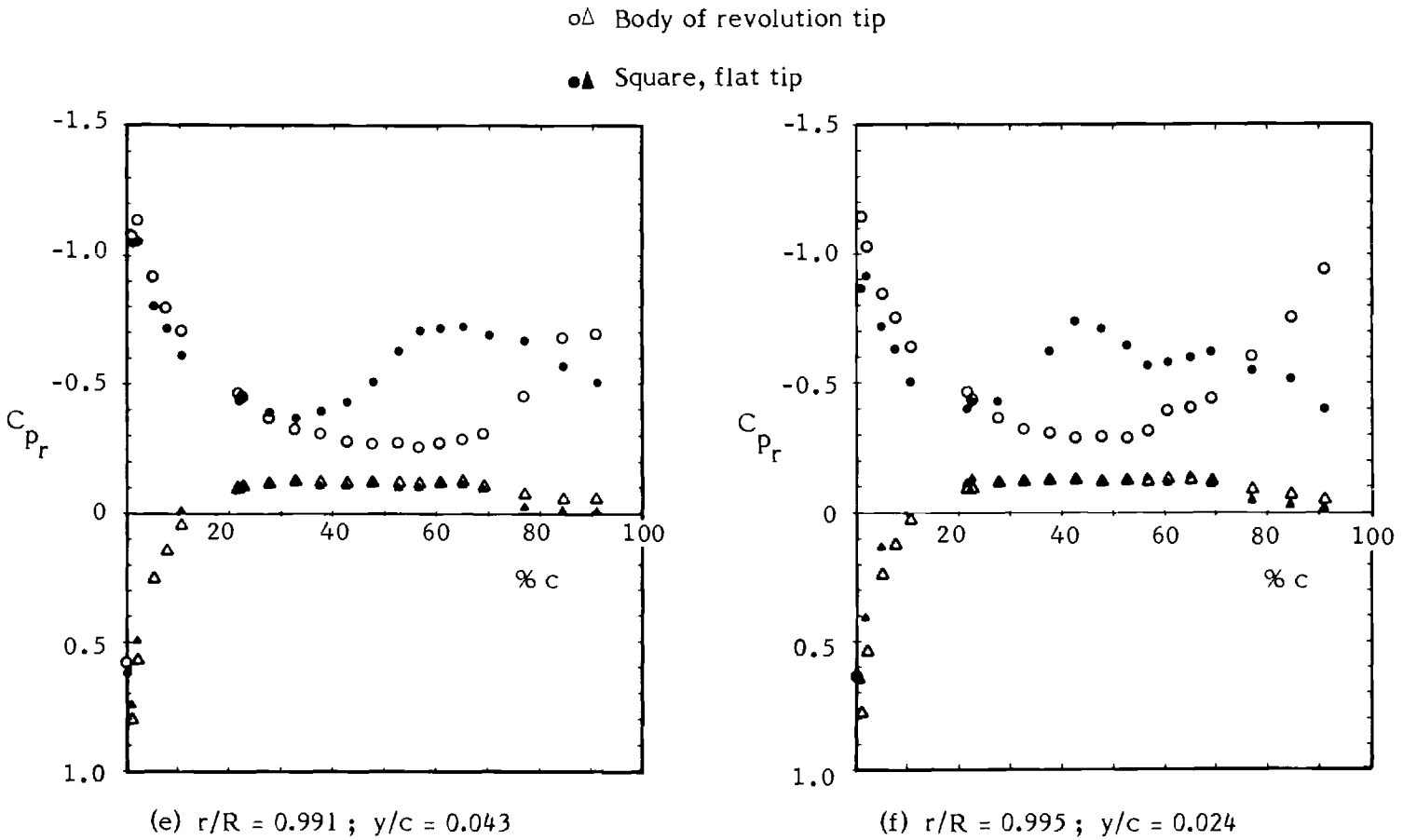

(e) r/R = 0.991 ; y/c = 0.043

(f) r/R = 0.995 ; y/c = 0.024

Figure 9. - (Concluded)

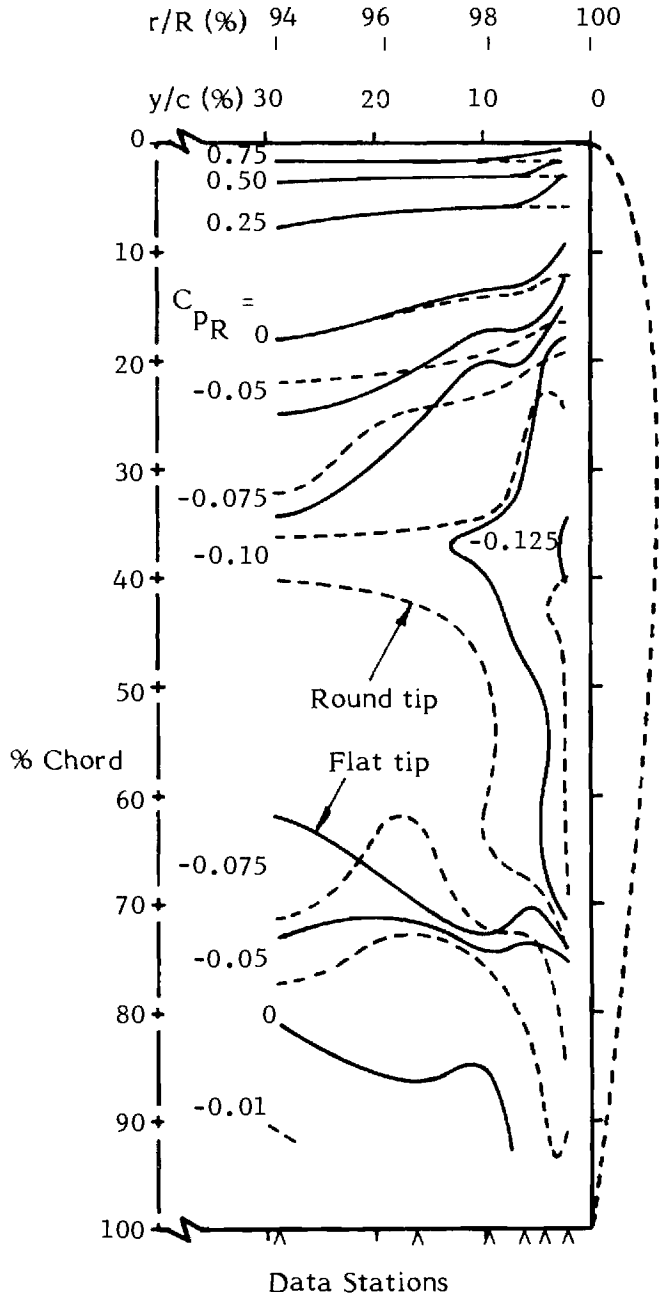

(a) Lower surface

Figure 10. - Blade pitch angle of 11.4 degrees. Comparison of contours of constant pressure coefficient based on tip speed as measured on a blade with a square, flat tip and on the same blade with a half-body of revolution tip.

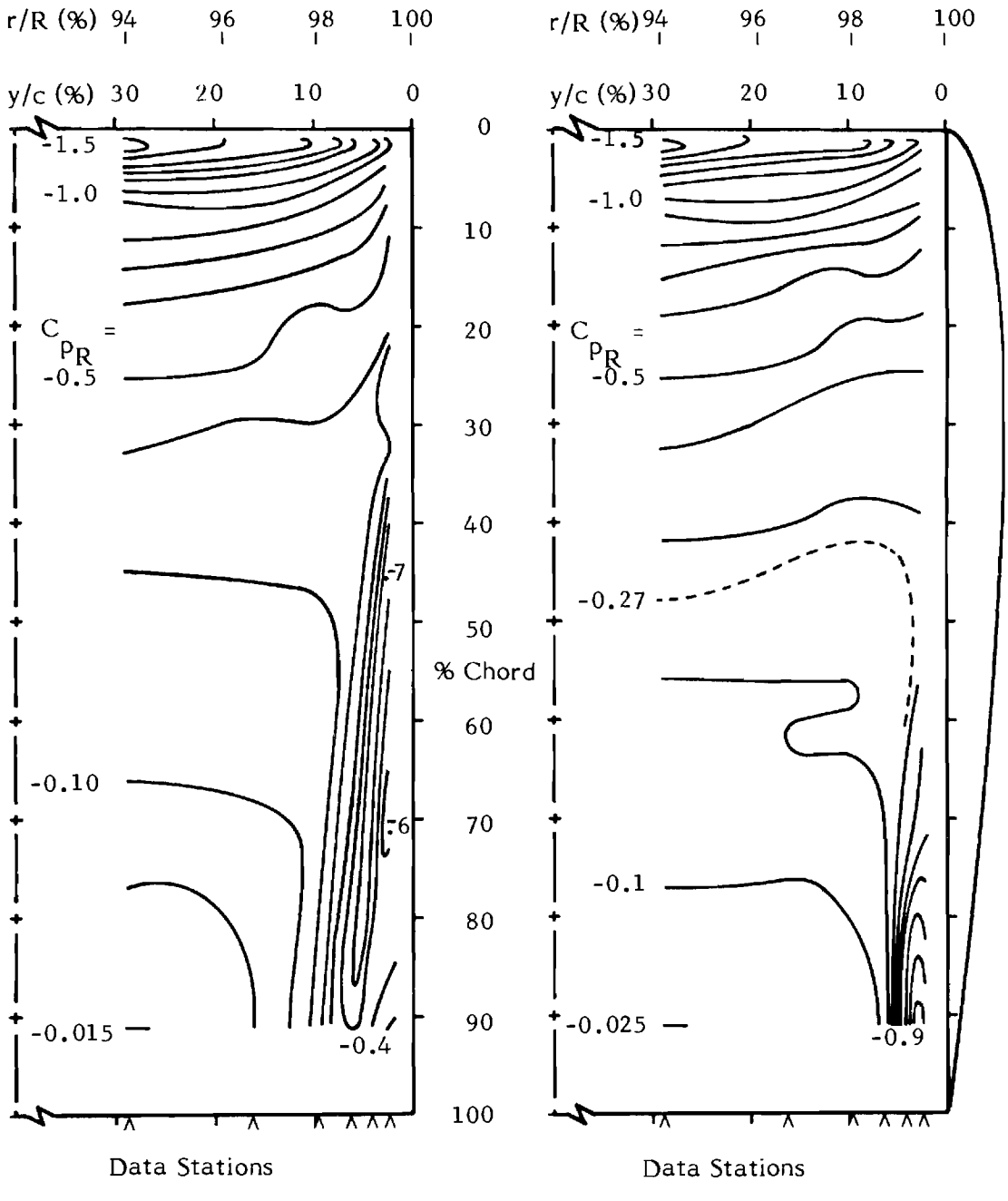

(b) Upper surface, flat tip

(c) Upper surface, round tip

Figure 10. - (Concluded)